Available online at www.sciencedirect.com
SCIENCE DIRECT®
Composites Science and Technology 65 (2005) 491–516
COMPOSITES SCIENCE AND TECHNOLOGY
www.elsevier.com/locate/compscitech

Review

Nanocomposites in context

Erik T. Thostenson, Chunyu Li, Tsu-Wei Chou *

Center for Composite Materials and Department of Mechanical Engineering, University of Delaware, 120 Spencer Lab., Newark, DE 19716, USA

Received 22 November 2004; accepted 22 November 2004
Available online 10 December 2004

Abstract

This paper provides an overview of recent advances in nanocomposites research. The key research opportunities and challenges in the development of structural and functional nanocomposites are addressed in the context of traditional fiber composites. The state of knowledge in processing, characterization, and analysis/modeling of nanocomposites is presented with a particular emphasis on identifying fundamental structure/property relationships. Critical issues in nanocomposites research as well as promising techniques for processing precursors for macroscopic nanocomposites are discussed.

Contents

* Corresponding author. Tel.: +1 302 831 2421; fax: +1 302 831 3619.
E-mail address: chou@me.udel.edu (T.-W. Chou).

0266-3538/$ - see front matter © 2004 Elsevier Ltd. All rights reserved.
doi:10.1016/j.compscitech.2004.11.003

1. Introduction

In 1985 Professor A. Kelly authored an article in *Composites Science and Technology* titled "Composites in Context" [1]. It was stated that, "The large scale social changes which influence the development of new materials are reviewed and the new materials and processing methods being developed in response to these are described and contrasted with some recent advances in composite materials science." Emerging technologies at the time included in situ metal–matrix composites, carbon-fiber-reinforced thermoplastic composites, SiC-reinforced aluminum as well as toughening of ceramics through the use of fiber-reinforcement. Tremendous developments have been made [2] in many aspects of composites research and technology during the two decades since the publication of Kelly's paper. Recent advances in producing nanostructured materials with novel material properties have stimulated research to create multi-functional macroscopic engineering materials by designing structures at the nanometer scale. Motivated by the recent enthusiasm in nanotechnology, development of nanocomposites is one of the rapidly evolving areas of composites research.

Nanotechnology can be broadly defined as, "The creation, processing, characterization, and utilization of materials, devices, and systems with dimensions on the order of 0.1–100 nm, exhibiting novel and significantly enhanced physical, chemical, and biological properties, functions, phenomena, and processes due to their nanoscale size" [3]. Current interests in nanotechnology encompass nano-biotechnology, nano-systems, nanoelectronics, and nano-structured materials, of which nanocomposites are a significant part.

Through nanotechnology, it is envisioned that nanostructured materials will be developed using a *bottom-up* approach. "More materials and products will be made from the bottom-up, that is, by building them from atoms, molecules, and the nanoscale powders, fibers and other small structural components made from them. This differs from all previous manufacturing, in which raw materials... get pressed, cut, molded and otherwise coerced into parts and products" [4].

Scientists and engineers working with fiber-reinforced composites have practiced this bottom-up approach in processing and manufacturing for decades. When designing a composite the material properties are tailored for the desired performance across various length scales. From selection and processing of matrix and fiber materials, and design and optimization of the fiber/matrix interface/interphase at the sub-micron scale to the manipulation of yarn bundles in 2-D and 3-D textiles to the lay-up of laminae in laminated composites and finally the net-shape forming of the macroscopic composite part, the integrated approach used in composites processing is a remarkable example in the successful use of the "bottom-up" approach.

The expansion of length scales from meters (finished woven composite parts), micrometers (fiber diameter), sub-micrometers (fiber/matrix interphase) to nanometers (nanotube diameter) presents tremendous opportunities for innovative approaches in the processing, characterization, and analysis/modeling of this new generation of composite materials. As scientists and engineers seek to make practical materials and devices from nanostructures, understanding material behavior across length scales from the atomistic to macroscopic levels is required. Knowledge of how the nanoscale structure influences the bulk properties will enable design of the nanostructure to create multi-functional composites.

The challenges in nanocomposites research perhaps can be best illustrated by the electron micrographs shown in Fig. 1 [5–7], where multi-walled carbon nano-

tubes (MWCNTs, 10–20 nm in diameter) have been deposited on the surface of carbon fibers (7 μm in diameter) in yarn bundles (measured in millimeters). When consolidated into a composite, the reinforcement scales span seven orders of magnitude. Fig. 2 shows a transmission electron microscope (TEM) image of the nanocomposite structure near the fiber/matrix interface, where the difference in reinforcement scale is readily apparent.

A morphological characteristic that is of fundamental importance in the understanding of the structure–property relationship of nanocomposites is the surface area/volume ratio of the reinforcement materials. This paper discusses nanocomposites based upon the three categories of reinforcement materials: particles (silica, metal, and other organic and inorganic particles), layered materials (graphite, layered silicate, and other layered minerals), and fibrous materials (nanofibers and nanotubes). As illustrated in Fig. 3, the change in particle diameter, layer thickness, or fibrous material diameter from micrometer to nanometer, changes the ratio by three orders in magnitude. At this scale, there is often distinct size dependence of the material properties. In addition, with the drastic increase in interfacial area, the properties of the composite become dominated more by the properties of the interface or interphase.

In this paper, we address the state of knowledge in processing, characterization, and analysis/modeling of nanocomposites with a particular emphasis on identifying fundamental structure/property relationships and compare the properties and performance of nanocomposites with traditional fiber composites.

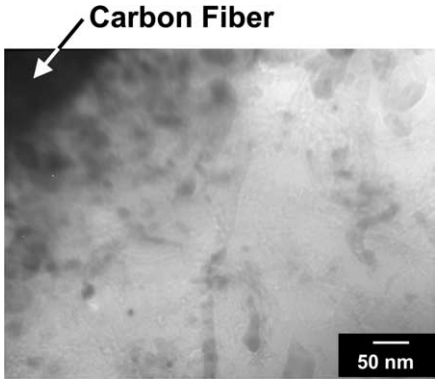

Fig. 2. TEM micrograph showing the nanotube composite structure directly adjacent to the carbon fiber/polymer matrix interface [6].

2. Nanoparticle-reinforced composites

Particulate composites reinforced with micron-sized particles of various materials are perhaps the most widely utilized composites in everyday materials. Particles are typically added to enhance the matrix elastic modulus and yield strength. By scaling the particle size down to the nanometer scale, it has been shown that novel material properties can be obtained. A few systems

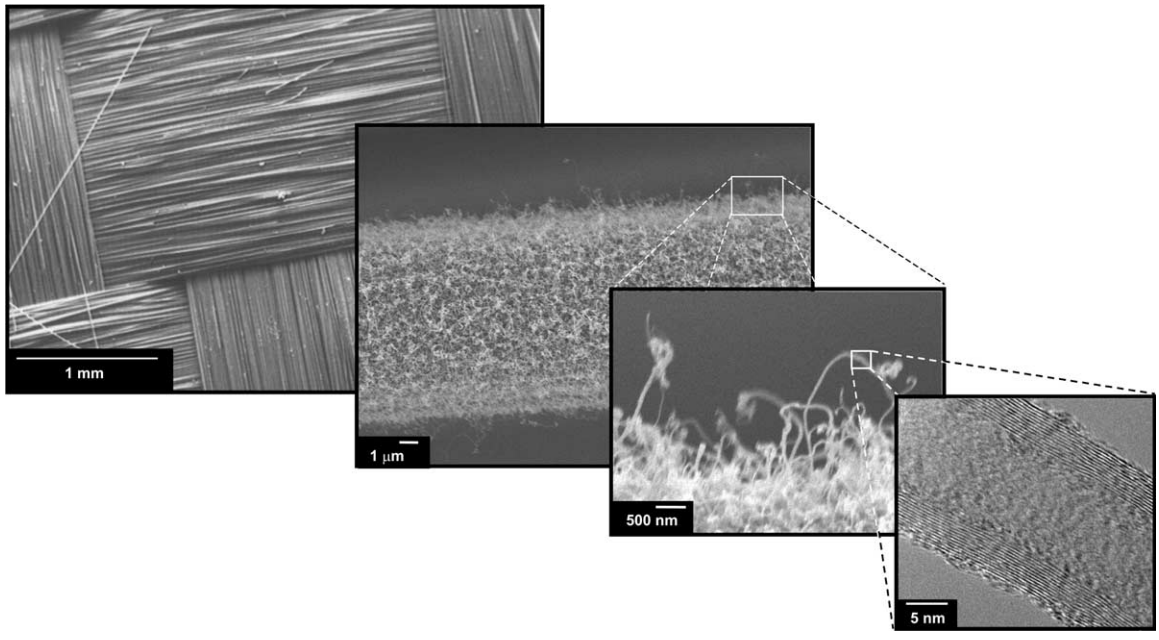

Fig. 1. Variation in reinforcement scales from millimeters to nanometers: (from left) from woven fabric of yarn bundles, to a single carbon fiber with entangled carbon nanotubes grown on the surface [5,6], to the nanometer diameter and wall structure of the carbon nanotube [7].

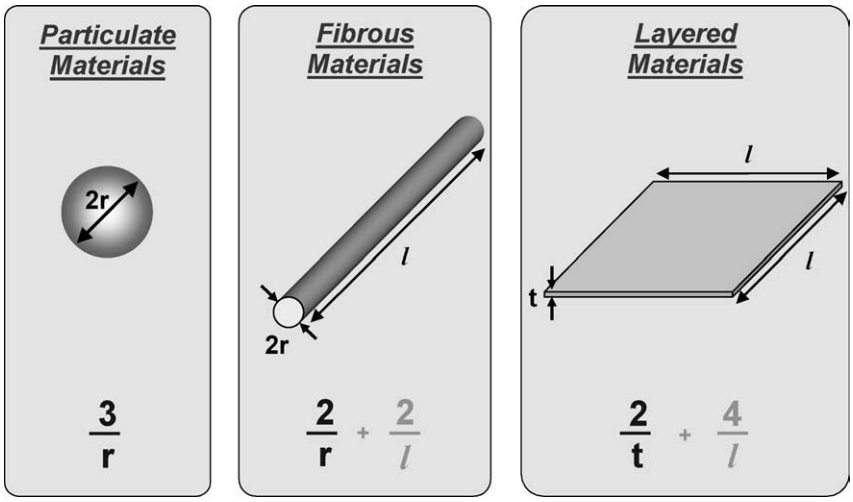

Fig. 3. Surface area/volume relations for varying reinforcement geometries.

are reviewed below for illustrating the resulting modification in matrix properties.

Micron-scale particles typically scatter light making otherwise transparent matrix materials appear opaque. Naganuma and Kagawa [8] showed in their study of SiO_2/epoxy composites that decreasing the particle size resulted in significantly improved transmittance of visible light. Singh et al. [9] studied the variation of fracture toughness of polyester resin due to the addition of aluminum particles of 20, 3.5 and 100 nm in diameter. Fig. 4 shows that the initial enhancement in fracture toughness is followed by decreases at higher particle volume fraction. This phenomenon is attributed to the agglomeration of nanoparticles at higher particle volume content.

Lopez and co-workers [10] examined the elastic modulus and strength of vinyl ester composites with the addition of 1, 2 and 3 wt% of alumina particles in the sizes of 40 nm, 1 μm and 3 μm. For all the particle sizes, the composite modulus increases monotonically with particle weight fraction. However, the strengths of composites are all below the strength of neat resin due to non-uniform particle size distribution and particle aggregation. The work of Thompson et al. [11] on metal oxide/polyimide nanocomposite films also noted similar difficulties in processing. Their study utilized antimony tin oxide (11–29 nm), indium tin oxide (17–30 nm) and yttrium oxide (11–44 nm) in two space-durable polyimides: TOR-NC and LaRC TMCP-2. The nanoscale additives resulted in higher stiffness, comparable or lower strengths and elongation, and lower dynamic stiffness (storage modulus). The dispersion of metal oxides on a nanometer scale was not achieved.

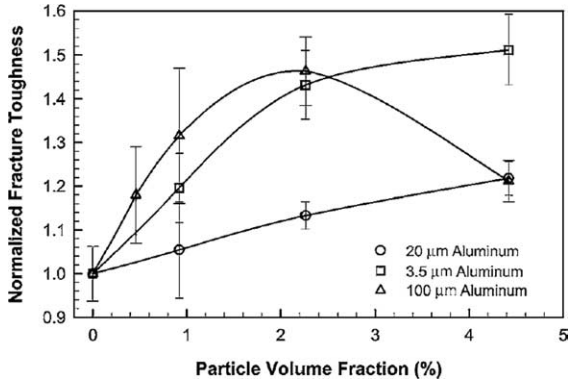

Fig. 4. Normalized fracture toughness with respect to volume fraction for various sized particles [9]. Reprinted with permission from [9]. Copyright (2002) Kluwer Academic Publishers.

Ash et al. [12] studied the mechanical behavior of alumina particulate/poly(methyl methacrylate) composites. They concluded that when a weak particle/matrix interface exists, the mode of yielding for glassy, amorphous polymers changes from cavitational to shear, which leads to a brittle-to-ductile transition. This behavior is attributed to increased polymer chain mobility, due to the presence of smaller particles, and also the capability to relieve tri-axial stress because of poorly bonded larger particles.

An extensive review of the structure–property relationships in nanoparticle/semi-crystalline thermoplastic composites has been made by Karger-Kocsis and Zhang [13].

3. Nanoplatelet-reinforced composites

Two types of nanoplatet-reinforced composites are reviewed: clay and graphite. In their bulk state, both clay and graphite exist as layered materials. In order to utilize these materials most efficiently, the layers must

be separated and dispersed throughout the matrix phase. The morphology of clay/polymer nanocomposites is illustrated in Fig. 5 [14]. In the conventional miscible state, the interlayer spacing in a clay particle is at its minimum. When polymer resin is inserted into the gallery between the adjacent layers, the spacing expands, and it is known as the intercalated state. When the layers are fully separated, the clay is considered to be exfoliated. Fig. 6 shows the TEM image of a montmorillonite poly (L-lactic acid) (PLLA) matrix nanocomposite, demonstrating intercalated and exfoliated clay layers [15].

Montmorillonite, saponite, and synthetic mica are commonly used clay materials, and developments in clay-based nanocomposites have been recently reviewed [16–18]. The advantages of polymer-based clay nanocomposites include improved stiffness, strength, toughness, and thermal stability as well as reduced gas permeability and coefficient of thermal expansion. Table 1 shows some properties of two commercially available clay particles with surface modifications [19,20]. The lack of affinity between hydrophilic silicate and hydrophobic polymer causes agglomeration of the mineral in the polymer matrix. Surface modification of clay particles facilitates the compatibility.

Table 2 illustrates the unique performance of Nylon-6/clay hybrid over a wide range of mechanical and thermal properties, as summarized by Okada and Usuki [20]. The pioneering work at Toyota Research Lab has clearly demonstrated that the addition of small amounts of montmorillonite clay material significantly enhances the tensile strength, tensile modulus, and heat degradation temperature (HDT), and reduces the rate of water absorption and CTE in the flow direction.

Table 3 summarizes the constituent properties of exfoliated clay [14,21,22]. Luo and Daniel [14] have modeled the Young's modulus of clay nanocomposites using a three-phase model: epoxy matrix, exfoliated clay nanolayer, and intercalated clay cluster (parallel platelet system). Fig. 7 shows that the experimental data lie within the upper (Voigt) and lower (Reuss) bond predictions and coincide fairly well with the Mori–Tanaka and Eshelby model predictions. The modeling work of Tsai and Sun [23] demonstrated that well dispersed platelets in the polymer matrix could significantly enhance the load transfer efficiency in these composites.

Fig. 8 compares the fracture toughness, K_{IC}, of epoxy matrix (DGEBA) composites reinforced with intercalated (ODTMA) and exfoliated (MT2EtOH) clay up to 10 vol%. Miyagawa and Drzal [21] attribute the high fracture toughness of intercalated clay composites to crack bridging by clay particles as well as crack deflection due to excellent adhesion of clay/epoxy interface and clay aggregate strength. On the other hand, the fracture of individual clay platelets in exfoliated clay

Fig. 6. TEM micrograph of a montmorillonite poly (L-lactic acid) nanocomposite, showing both intercalated and exfoliated states [15]. Reprinted with permission from [15]. Copyright (2003) American Chemical Society.

Table 1
Properties of clay platelets [19,20]

Physical properties	Closite® 30B	Nanomer 1.28E
Color	Off white	White
Density (g/cm^3)	1.98	1.90
D-spacing ($D_{0\,0\,1}$), Å	18.5	>20
Aspect ratio	200–1000	200–500
Surface area (m^2/g)	750	750
Mean particle size (μm)	6	8–10

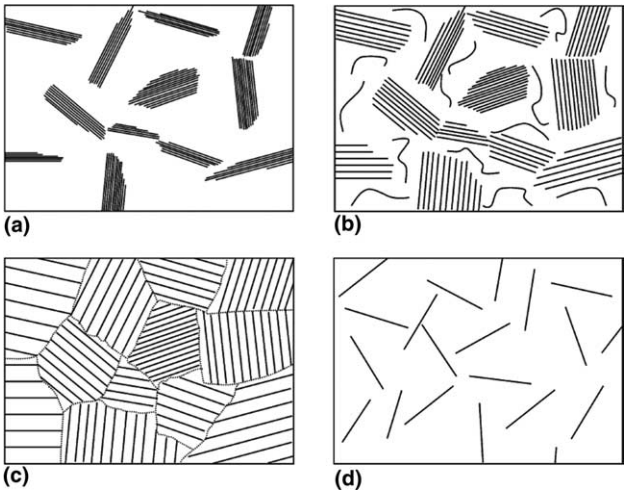

Fig. 5. Morphologies of polymer/clay nanocomposites: (a) conventional miscible, (b) partially intercalated and exfoliated, (c) fully intercalated and dispersed and (d) fully exfoliated and dispersed [14].

Table 2
Properties of Nylon-6/clay nanocomposites [20]

Sample	Wt% clay *Montmorillonite*	Tensile strength (MPa)	Tensile modulus (GPa)	Charpy impact strength (kJ/m^3)	HDT at 18.5 kg cm^{-2} (°C)
NCH-5	4.2	107	2.1	2.1	152
NCC-5	5.0	61	1.0	1.0	89
Nylon-6	0	69	1.1	1.1	65

Sample	Wt% clay *Montmorillonite*	Rate of water absorption 25 °C, 1 day	CTE (°C × 10^{-5})	
			Flow direction	Perpendicular direction
NCH-5	4.2	0.51	6.3	13.1
NCC-5	5.0	0.90	10.3	13.4
Nylon-6	0	0.87	11.7	11.8

Table 3
Properties of exfoliated graphite platelets as compared to exfoliated clay platelets

	Graphene sheet[a]	Clay platelet[b,c]
Physical structure	~1 nm × 100 nm	~1 nm × 1000 nm
Tensile modulus (GPa)	1,000	170
Tensile strength (GPa)	10–20	1
Resistivity (Ω cm)	~50 × 10^{-6}	10^{10}–10^{16}
Thermal conductivity (W/m K)	3000	0.67
CTE	~1 × 10^{-6}	8–16 × 10^{-6}
Density (g/cm^3)	2.0	2.5–3.0
D-spacing (nm)	0.34	1.85

[a] Fukushima and Drzal [22].
[b] Miyagawa and Drzal [21].
[c] Luo and Daniel [14].

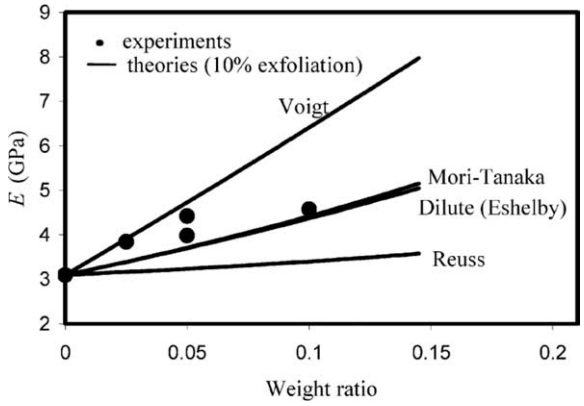

Fig. 7. Comparison of theoretical models with experimental data for nanocomposite elastic modulus [14].

composites leads to less rough fracture surface and lower fracture toughness.

In addition to mechanical properties, the thermal stability, fire resistance and gas barrier properties of polymer/clay nanocomposites can be enhanced through the addition of nanometer-scale reinforcement. For example, Ogasawara et al. [24] have investigated the helium permeability of nanoclay for potential applications in liquid hydrogen tanks and fuel cells. The addition of nanoclay to the epoxy resin substantially decreased the

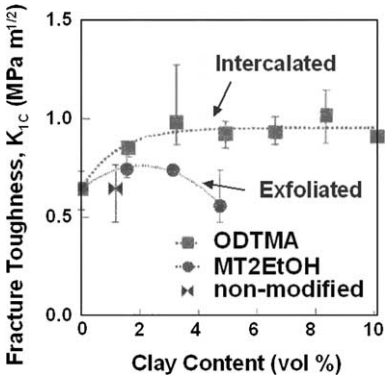

Fig. 8. Influence of clay content and exfoliation on fracture toughness [21].

gas diffusivity as compared with unreinforced epoxy. The results are consistent with the Hatta-Taya theory and it was revealed that the dispersion of platelets is more effective than spherical or fiber-like reinforcement in improving the nanocomposite barrier properties.

Regarding the other layered material, the exfoliated graphite or graphene sheet has about the same thickness as exfoliated clay. Table 3 shows their high tensile modulus, tensile strength, thermal conductivity, and low electrical resistivity, comparing to clay platelets. The low electrical resistivity of exfoliated graphite facilitates the conductivity of polymer composites when a threshold percolation weight content of the conductive phase is reached. Fig. 9 shows the results of Fukushima and Drzal [22] on the resistivity of epoxy matrix (EPON 828) composites with the addition of vapor grown carbon fiber (VGCF), carbon black, PAN carbon fiber, exfoliated graphite and milled graphite. The graphite nanoplatelets are treated in O_2 plasma for initiating radical polymerization. The percolation threshold for exfoliated graphite is around 1 wt%. Zheng and co-workers [25,26] have also reported reduced percolation thresholds in exfoliated graphite nanoplatelet/thermoplastic composites.

Song et al. [27] have modeled the von Mises stress distribution in graphite/PAN nanocomposites with respect

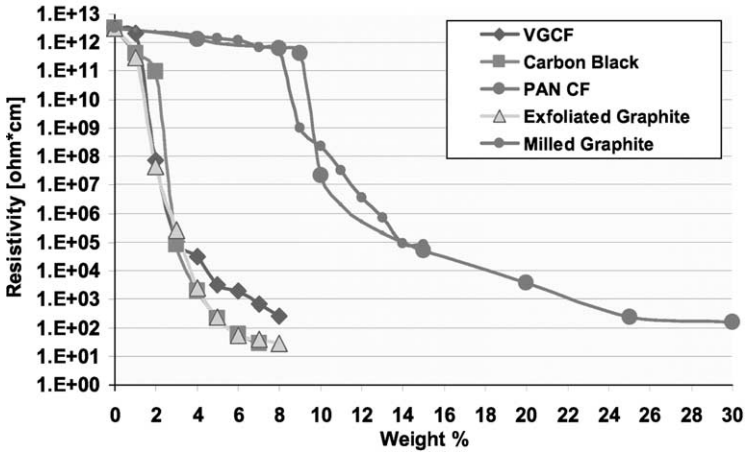

Fig. 9. Comparison of various carbon reinforcement materials on the composite bulk resistivity [22].

to the level of exfoliation. They demonstrated the reduction in the magnitude of stress concentration with layer thickness at the tip of graphite layers, aligned with the axial tensile load. Such conclusion is similar to those obtained for short fiber composites where the dispersion of a fiber bundle has the benefit of reducing the stress concentration in the matrix material at the bundle ends and thus, the chance of matrix cracking or plastic deformation.

The greatly enhanced electrical conductivity of polymeric material with the addition of small amount of graphite platelets has found many practical applications. These include EMI shielding and heat management of electronic and computer devices or equipment, electrostatic paint for automobiles and polymer sheath of electric cables [23].

Nanoclay/polypropylene composites are being used as functional parts in automobiles. For instance, General Motors (GM) is using about 660,000 lbs of nanocomposite material per year.

4. Nanofiber-reinforced composites

Vapor grown carbon nanofibers (CNF) have been used to reinforce a variety of polymers, including polypropylene, polycarbonate, nylon, poly(ether sulfone), poly(ethylene terephthalate), poly(phenylene sulfide), acrylonitrile-butadiene-styrene (ABS), and epoxy. Carbon nanofibers are known to have wide-ranging morphologies, from structures with a disordered bamboo-like structure [28] (Fig. 10(a)) to highly graphitized "cup stacked" structures [29,30] (Figs. 10(b) and (c)), where the conical shells of the nanofiber are nested within each other. Carbon nanofibers typically have diameters on the order of 50–200 nm. Wei and Srivastava [31] have modeled the mechanical properties of carbon nanofibers with varying morphology using continuum elastic theory and molecular dynamics simulations. The axial Young's modulus of the nanofiber is particularly sensitive to the shell tilt angle, where fibers that have small tilt angles from the axial direction show much higher Young's modulus than fibers with large tilt angles. The wide-ranging morphology of the carbon nanofibers and their associated properties results in a broad range of scatter for experimental results on processing and characterization of nanofiber composites.

Finegan and co-workers [32,33] have investigated the processing and properties of carbon nanofiber/polypropylene nanocomposites. In their work, they used a variety of as-grown nanofibers. Carbon nanofibers that were produced with longer gas phase feedstock residence times were less graphitic but adhered better to the polypropylene matrix, with composites showing improved tensile strength and Young's modulus. Oxidation of the carbon nanofiber was found to increase adhesion to the matrix and increase composite tensile strength, but extended oxidation reduced the properties of the fibers and their composites. In their investigation on the nanofiber composite damping properties, Finegan et al. [33] concluded that the trend of stiffness variation with fiber volume content is opposite to the trend of loss factor and damping in the composite is matrix-dominated.

Ma and co-workers [34] and Sandler et al. [35] have spun polymer fibers with carbon nanofibers as reinforcement. Ma et al. utilized a variety of techniques to achieve dispersion of carbon nanofibers in a poly(ethylene terephthalate) (PET) matrix and subsequently melt-spun fibers. The compressive strength and torsional moduli of the nanocomposite fibers were considerably higher than that for the unreinforced PET fiber. Sandler et al. [35] produced fibers from semicrystalline high-performance poly(ether ether ketone) (PEEK) containing up to 10 wt% vapor-grown carbon nanofibers. Their experimental results highlight the need to characterize

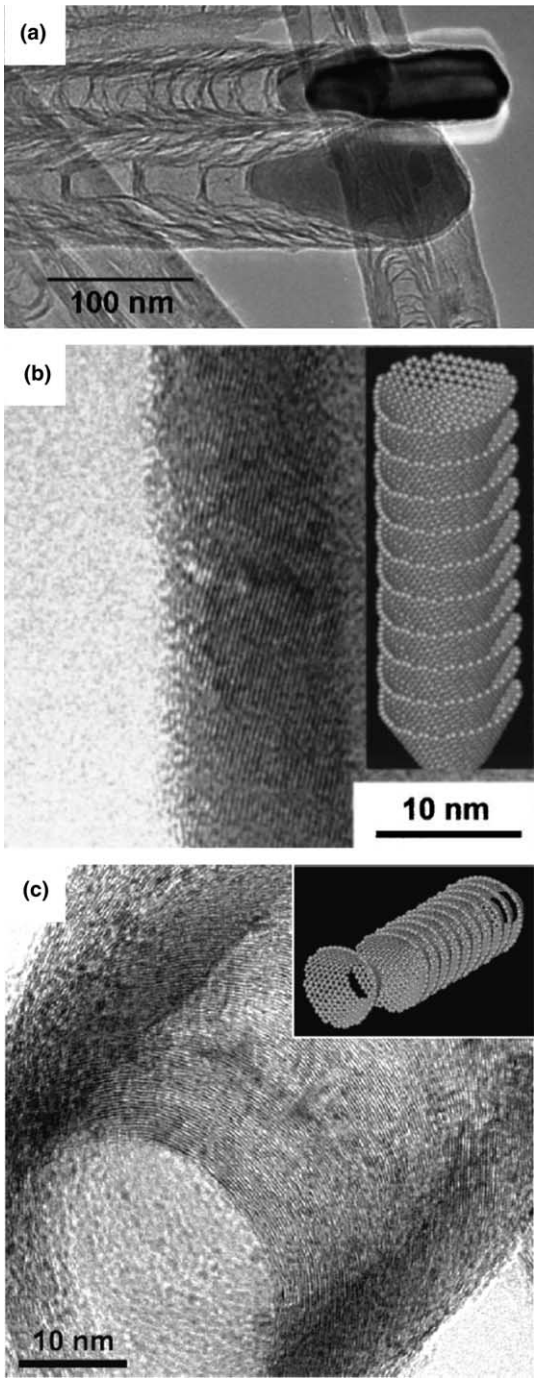

Fig. 10. TEM micrographs of the nanoscale structure of carbon nanofibers showing: (a) disordered bamboo-like structures [28], (b) highly graphitized sidewall of a cup-stacked (molecular models inset) nanofibers showing the shell tilt angle [29] and (c) a nesting of the stacked layers [30]. Reprinted with permission from [30]. Copyright (2003) American Chemical Society.

both the crystalline matrix morphology and nanocomposite structure when evaluating performance. This is crucial to understanding the intrinsic properties of the nanoscale reinforcement.

Many of the key challenges associated with the processing, characterization, and modeling of carbon nanofiber composites, such as dispersion and adhesion, are similar to those for nanotube-reinforced composites and are discussed in the following section.

5. Carbon nanotube-reinforced composites

As reviewed by Thostenson et al. [36], the morphology of a carbon nanotube is defined by the orientation and magnitude of the chiral vector in a grephene sheet, which is "wrapped up" to form the single-walled carbon nanotube (SWCNT). The two limiting configurations are armchair and zigzag nanotubes (Fig. 11).

Since their observation over a decade ago [37], numerous investigators have reported remarkable physical and mechanical properties of carbon nanotube. Below is a summary of these exceptional properties excerpted from Collins and Avouris [38]. The density of a SWCNT is about 1.33–1.40 g/cm^3, which is just one-half of the density of aluminum. The elastic modulus of SWCNT is comparable to that of diamond (1.2 TPa). The reported tensile strength of SWCNT is much higher than that of high-strength steel (2 GPa). The tremendous resilience of SWCNT in sustaining bending to large angles and restraightening without damage is distinctively different from the plastic deformation of metals and brittle fracture of carbon fibers at much lower strain when subjected to the same type of deformation. The electric current carrying capability is estimated to be 1×10^9 amp/cm^2, whereas copper wires burn out at about 1×10^6 amp/cm^2. The thermal conductivity of SWCNT is predicted to be 6000 W/m K at room temperature; this is nearly double the thermal conductivity of diamond of 3320 W/m K. SWCNTs are stable up to 2800 °C in vacuum and 750 °C in air, whereas metal wires in microchips melt at 600–1000 °C. SWCNTs have great potential in field emission applications because they can activate phosphors at 1–3 V if electrodes are spaced 1 μm apart. Traditional Mo tips require fields of 10–100 V/μm and have very limited lifetimes.

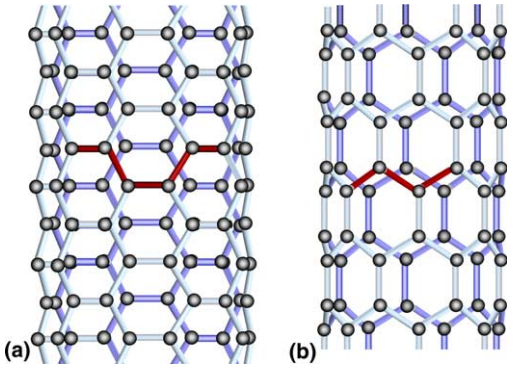

Fig. 11. Atomic structures of (a) armchair and (b) zig-zag carbon nanotubes [36].

The outstanding thermal and electric properties combined with their high specific stiffness and strength, and very large aspect ratios have stimulated the development of nanotube-reinforced composites for both *structural* and *functional* applications [36,39,40].

5.1. Carbon nanotube morphology

Carbon nanotubes have been fabricated by a variety of techniques [36]. The morphology of nanotubes exhibits a great degree of variability. Furthermore, in spite of our knowledge in general regarding the exceptional properties measured and predicted to date, our ability in applying carbon nanotubes to structural and functional composites is handicapped by the lack of a comprehensive grasp of the basic and precise knowledge of their properties. The brief review of the morphology and properties given in this sub-section serves to exemplify such variability.

First, regarding the morphology of SWCNTs, the variability could include the nanotube length, diameter and chirality as well as the tube-end configuration (end-caps). The variability in morphology is much more pronounced in a MWCNT, which can be considered as composed of nested SWCNTs. The major additional structural parameters include nanotube outer and inner diameter, number of nested SWCNTs (wall thickness), and growth-induced configuration, such as bamboo structures.

To demonstrate the structural variability of MWCNTs, Thostenson and Chou [7] have utilized high-resolution TEM micrographs taken of the CVD-grown tubes and image analysis software to measure the structural dimensions for quantifying both the distribution of nanotube diameter and the nanotube wall structure. To obtain statistically meaningful data nearly 700 nanotubes of the same batch were examined. Fig. 12 shows a TEM micrograph of a MWCNT, indicating the outer (d) and inner (d_i) diameter as well as a histogram for the nanotube outside diameter distribution, which is a bimodal distribution with peaks near 18 and 30 μm.

In order to obtain a probability density function for the nanotube diameter distribution, Thostenson and Chou [7] fitted the data of Fig. 12 to double Lorentzian distribution and double Gaussian distributions. For small-diameter nanotubes, the Gaussian curve most accurately fit the data, but for large-diameter nanotubes, the Gaussian curve underestimates the amount of nanotubes. The volume distribution of the nanotubes is obtained from the diameter distribution functions.

Although the large-diameter nanotubes are of a relatively small percentage of the total number of nanotubes, they occupy a significant percentage of volume within the composite. The more accurate modeling of the volume distribution by the Lorentzian curve at large nanotube diameter is crucial because the volume occupied by a given nanotube in the composite varies with d^2.

The wall thickness of the same MWCNTs as in Fig. 12 are presented in Fig. 13(a) as a function of nanotube diameter. A strong linear relationship between the nanotube diameter and wall thickness is observed. The nanoscale tubular structure of the MWCNTs also results in a distribution of nanotube density. From the measurement of inside and outside diameter, the nanotube density per unit length can be calculated by assuming that the graphite layers of the tube shell have the density of fully dense graphite ($\rho_g = 2.25$ g/cm^3). The nanotube density as a function of diameter is shown in Fig. 13(b), where the curved line is obtained directly from the straight line in Fig. 13(a).

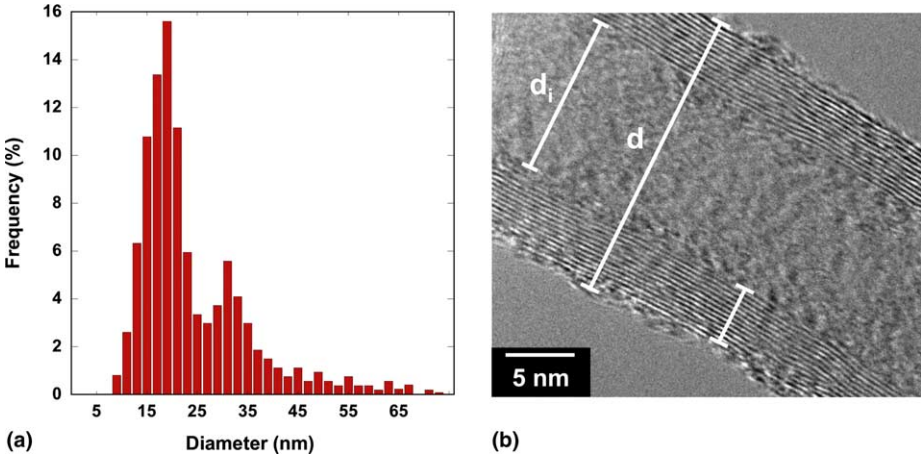

Fig. 12. (a) Diameter distribution of CVD-grown multi-walled carbon nanotubes taken from measurements of (b) TEM micrographs [7].

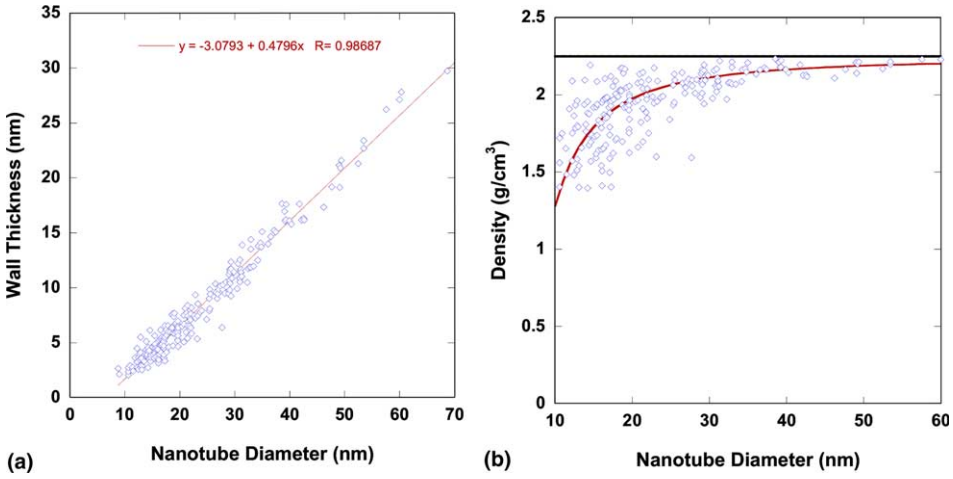

Fig. 13. Variation in: (a) nanotube wall thickness with nanotube diameter and (b) density with nanotube diameter [7].

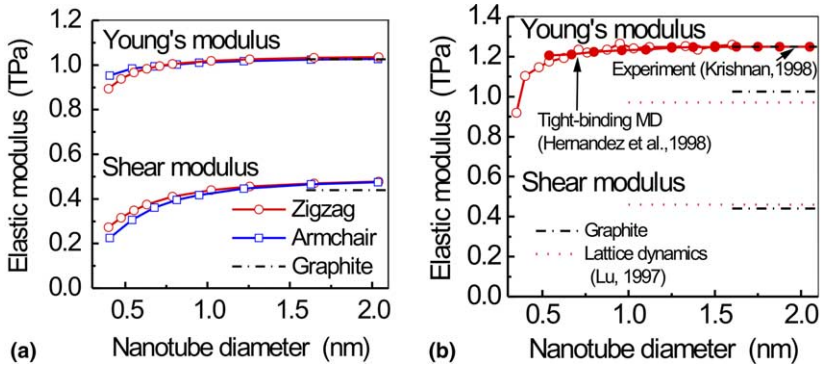

Fig. 14. Diameter sensitivity of elastic modulus: (a) predicted by molecular structural mechanics and Li and Chou [43] and (b) other methods (Hernandez et al. [44]; Lu [45]; Krishnan [46]).

5.2. Elastic and strength properties of carbon nanotubes

The elastic and strength properties of SWCNT and MWCNTs have been extensively studied both analytically and experimentally. Review articles on these subjects can be found, for example, in Thostenson et al. [36], Qian et al. [41] and Srivastava et al. [42]. The following brief summary not only presents some recent results but also illustrates the variability of results obtained from analytical predictions as well as experimental measurements. Such variability poses considerable uncertainty in utilizing the elastic modulus and strength data in micromechanical models for composites.

Fig. 14(a) gives the axial tensile Young's modulus and shear modulus as functions of SWCNT diameter, which were obtained by Li and Chou [43] using the molecular structural mechanics approach. The results are sensitive to nanotube diameter and nanotube structure at small diameter. The axial Young's modulus approaches to 1.03 TPa for diameters $\geqslant$1.0 nm, while the shear modulus is about 0.5 TPa for diameters >1.25 nm. Both the Young's modulus and shear modulus values approach to the corresponding values of graphite at large tube diameter. Fig. 14(b) shows the nanotube diameter dependence of axial modulus predicted by Hernandez et al. [44] using tight-binding molecular dynamics, and the shear modulus predictions of Lu [45] based on lattice dynamics. Besides the axial Young's modulus and shear modulus, the transverse Young's moduli of SWCNTs and double-walled carbon nanotubes (DWCNT) have been studied using the molecular structural mechanics method [47]. The variations of Poisson's ratio of SWCNTs with the tube diameter predicted by the molecular structural mechanics approach of Li and Chou are shown to depend strongly on both nanotube diameter and chirality (Fig. 15). The results of Hernandez et al. [44], Lu [45], and Sanchez-Portal et al. [48] on the other hand, are nearly insensitive to tube diameter. The recent results of the axial Young's modulus of carbon nanotubes are summarized in Table 4 [43,45,49–55].

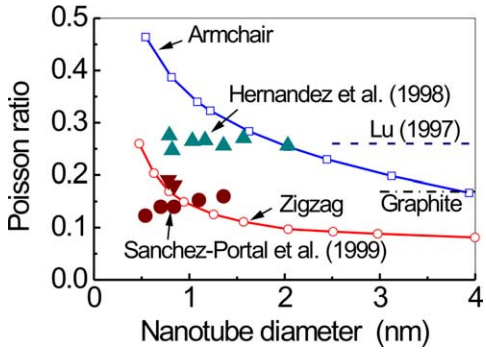

Fig. 15. Poisson's ratio predicted by molecular structural mechanics of Li and Chou and other methods (Hernandez et al. [44]; Lu [45]; Sanchez-Portal et al. [48]).

Table 4
Experimental and theoretical results for nanotube axial Young's modulus

Elastic modulus (TPa)	Method of measurement
Experimental measurements	
1.26 (±20%)	TEM – thermal vibration of a beam [49]
1.28 (±40%)	AFM – 1 end clamped [50]
0.81 (±50%)	AFM – 2 ends clamped [51]
0.1–1.0 (±30%)	TEM – electrostatic deflection [52]
0.27–0.95	Dual AFM cantilevers [53]
0.91 (±20%)	TEM – direct tension [54]
	Method of calculation
Theoretical calculations	
0.97	Empirical lattice dynamics [45]
1.0 (±15%)	*Ab initio* [47]
1.05 (±5%)	Molecular structural mechanics [43]
0.68	Pin-jointed Truss model [55]

Large variability exists in both experimental and analytical findings.

To illustrate the load-sharing characteristics of MWCNTs, the modeling works of Li and Chou [56] for a DWCNT is recapitulated below. To delineate the effect of van der Waals forces in the deformation of MWCNT, a two-layer MWCNT under two different tensile loading conditions is examined in their work. One loading condition assumes that uniform forces are applied only on atoms at the end of the outer layer, while in the other loading condition, uniform forces are applied on atoms at the end of both inner and outer layers. In both loading conditions, the atoms at the end of the outer layer reach nearly the same displacement. But the displacements of the atoms at the end of the inner layer show a large difference in the two loading conditions. When the forces are applied only on the outer layer, the inner layer exhibits small axial displacements. This means that the force acting on the outer layer is barely transferred to the inner layer through van der Waals interactions. This finding is consistent with the experimental observation that deformation of MWCNTs often leads to the separation and pullout of the individual layers [53].

Table 5
Experimental and theoretical results for nanotube axial strength

Axial strength (GPa)	Method of measurement
Experimental measurements	
13–52	Dual AFM cantilivers, SWCNT bundles [53]
11–63	Dual AFM cantilivers, MWCNTs [57]
45 (±7)	AFM – lateral force mode, MWCNTs [58]
150 (±30%)	TEM – direct tension, MWCNTs [54]
	Method of calculation
Theoretical calculations (SWCNT)	
150	Molecular dynamics simulation [59]
93–112	Molecular mechanics simulation [60]

The tensile strength data of carbon nanotubes are summarized in Table 5 [53,57–60]. A variety of techniques have been adopted for measuring the strength of SWCNT bundles and MWCNTs. Again, there exists large variability in the measured and predicted strength values.

By employing the molecular structural mechanics, Li and Chou [61,62] studied the free vibrations of carbon nanotubes and predicted that the fundamental frequencies of cantilevered or bridged SWCNTs as nanomechanical resonators could reach the level of 10 GHz–1.5 THz. The effects of tube diameter, length, and end constraints on the fundamental frequency have been discerned. Furthermore, the fundamental frequencies of DWCNTs are about 10% lower than those of SWCNTs of the same outer diameter. The non-coaxial vibration of double-walled nanotubes begins at the third resonant frequency. The potential of carbon nanotubes for mass sensing, strain sensing and pressure sensing has been explored by Li and Chou [63,64].

5.3. Carbon nanotube/polymer composites

Both SWCNTs and MWCNTs have been utilized for reinforcing thermoset polymers (epoxy, polyimide, and phenolic), as well as thermoplastic polymers (polypropylene, polystyrene, poly methyl methacrylate (PMMA), nylon 12, and poly ether ether ketone (PEEK)). Several composite systems are reviewed below.

Tai et al. [65] have processed a phenolic-based nanocomposite using MWCNTs, which were synthesized through the floating catalyst chemical vapor deposition process with tube diameter < 50 nm and length > 10 μm. SEM images of brittle tensile fracture surfaces show fairly uniform nanotube distribution and nanotube pull-out. Enhancement in Young's modulus and strength due to the addition of nanotubes was reported.

Gojny and co-workers [66] fabricated nanocomposites consisting of DWCNTs with a high degree of dispersion.

The resulting composites showed increase of strength, Young's modulus and strain to failure at a nanotube content of only 0.1 wt%. In addition, the nanocomposites showed significantly enhanced fracture toughness as compared to the unreinforced epoxy.

Ogasawara et al. [67] reinforced a phenylethyl terminated polyimide with MWCNTs, which are a few hundred μm in length and 20–100 nm in diameter. The composites were made by mechanical blending of the nanotubes in the matrix, melting at 320 °C, and curing at 370 °C under 0.2 MPa pressure. The resulting elastic and mechanical properties are shown in Table 6. The addition of MWCNTs enhances the tensile Young's modulus, and reduces the tensile strength and ultimate strain.

Thostenson and Chou [7,68] have characterized the nanotube structure and elastic properties of a model composite system of aligned MWCNTs embedded in a polystyrene matrix. In this work, a micro-scale twin-screw extruder was utilized to obtain high shear mixing necessary for disentangling the CVD-grown MWCNTs, and disperse them uniformly in a polystyrene thermoplastic matrix. The polymer melt was then extruded through a rectangular die and drawn under tension before solidification. The process of extruding the nanocomposite through the die and subsequent drawing results in a continuous ribbon of aligned nanocomposites. Fig. 16(a) shows a TEM micrograph of the as-processed 5-wt% nanocomposite film showing large-scale dispersion and alignment of carbon nanotubes in the polymer matrix. The arrow in Fig. 16(a) indicates the direction of alignment taken as the principal material direction with a nanotube orientation of 0°. The grey lines perpendicular to the arrow in the TEM micrograph are artifacts from microtome cutting process. Fig. 16(b) shows the distribution of nanotube alignment from the image analysis. Based on the data, the standard deviation of nanotube alignment from the principal material direction is less than ±15°.

The axial elastic properties of the MWCNT/polystyrene system have been modeled by Thostenson and Chou [7] using a "micromechanics" approach through defining an equivalent effective fiber property for the diameter-sensitive carbon nanotube elastic modulus. To accurately model the elastic properties of the composite, the contribution to the overall elastic modulus of each nanotube diameter, and the volume fraction that tubes of a specific diameter occupy within the composite have been taken into account. Using the knowledge of the tube diameter distribution functions as well as the nanotube density and volume distribution as functions of tube diameter, the micromechanics approach identifies the correlation between axial Young's modulus, and the diameter, volume fraction and length of nanotubes of the aligned nanocomposite model system.

Table 6
Properties of CNT/polyimide nanocomposites [67]

CNT (wt%)	CNT (vol%)	T_g[a] (°C)	E[b] (GPa)	σ_{uts} (MPa)	ε_{max} (%)	$\sigma_{0.2}$ (MPa)
0	0	335	2.84	115.6	7.6	69.8
3.3	2.3	339	3.07	99.5	4.0	80.5
7.7	5.4	350	3.28	97.6	3.6	84.6
14.3	10.3	357	3.90	95.2	2.6	92.6

[a] Onset temperature of decrease in storage modulus (DMA).
[b] Strain range of 0.5–1.0% (tensile testing).

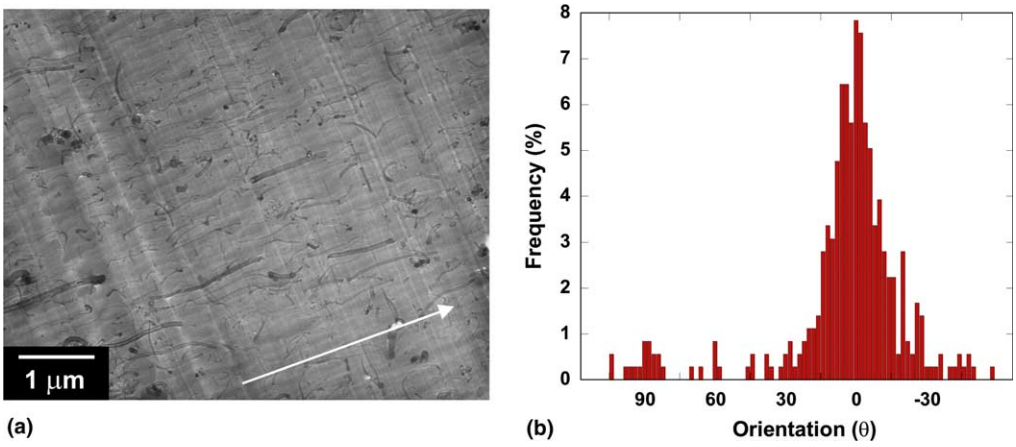

Fig. 16. (a) TEM micrograph of process-induced orientation in nanocomposite ribbons [68] and (b) image analysis of orientation distribution [7].

Experiments by Frogley et al. [69] on silicone-based elastomers reinforced with SWCNTs have shown significant increases in the initial modulus of the composites, accompanied by a reduction in the ultimate properties. Raman spectroscopy experiments show a loss of stress transfer to the nanotubes at around 10–20% strain, suggesting the break-down of the effective interface between the phases. On the other hand, the reorientation of the nanotubes under strain in the samples may be responsible for the initial increase in modulus enhancement under strain.

More recently, experiments on silicone elastomer-reinforced with SWCNTs have shown significant increase in stiffness and strength. However, the relative magnitudes of the improvement decreased with higher nanotube volume loading because the composite became more brittle [70].

5.4. Interfaces in carbon nanotube/polymer composites

In the processing of nanocomposites, carbon nanotubes need to be separated from bundles and dispersed uniformly in a polymer matrix for maximizing their contact surface area with the matrix. Modification of nanotube surfaces, for example, the creation of covalent chemical bonds between nanotubes and the polymer matrix, enhances their interactions and gives rise to higher interfacial shear strength than van der Waals bonds [36,71]. Sinnott [72] has provided an in-depth review of the chemical functionalization of carbon nanotubes, where the chemical bonds are used to tailor the interaction of the nanotube with the other entities, such as a solvent, a polymer matrix or other nanotubes. The two major approaches to functionalization are chemical methods and irradiation with electrons or ions. Brief excerpts from Sinnott [72] are given below, and a few examples concerning modification of nanotube/polymer interface in composites are also given.

The chemical methods involve the attachment of chemical bonds to either the nanotube ends or sidewalls. First, nanotube caps, which are more reactive because of their high degree of curvature can react with a strong acid. The open ends can be stabilized by carboxylic acid and hydroxide groups. In the work of Liu et al. [73], sonication of purified SWCNTs in a mixture of concentrated sulfuric and nitric acid cuts the tube into short segments with open ends, about 300 nm in length, with carboxylic acid (–COOH) groups covalently attached to the openings. The mechanism involves the oxidation of the nanotube walls at defect sites. As reviewed by Sinnott [72], functionalized short SWCNTs could be made soluble in water or organic solvents. Longer, micrometer-length SWCNTs can be made soluble in organic solvents through ionic functionalization of the carboxylic acid groups.

A recent example of functionalization at nanotube ends for the preparation of SWCNT-reinforced polymer composites can be found in the work of Sen et al. [74] and Hamon et al. [75]. In their study of the effect of interfacial reaction between SWCNTs and the polyurethane matrix, ester-functionalized SWCNTs, SWCNT-$COO(CH_2)_{11}CH_3$, were synthesized and electrospun with polyurethane. According to Sen et al. [74], the chemical functionalization is an effective approach to exfoliate the SWCNT bundles and improve the processability of SWCNTs. The ester form of SWCNTs has been shown to be easily dispersed in organic solvent as both individual nanotubes and small bundles of 2–5 nanotubes. The improved chemical compatibility and dispersion of the functionalized nanotubes within the polyurethane matrix enables a significant enhancement in the tensile strength and tangent modulus of the composite membrane fabricated by electrospinning when compared to the pure polymer membrane.

Covalent chemical functionalization of the nanotube sidewalls has also been achieved. Nanotube walls can be modified by reactive elements, such as fluorine. Fluorine chemically binds to, or functionalizes, the nanotube walls at room temperature and produces severe modification of the nanotube's tubular structure at temperatures of 500–600 °C [72]. Nanotube sidewalls can also be functionalized through non-covalent interaction through the irreversible adsorption of a bifunctional molecule onto the surface of a SWCNT in an organic solvent [72,76]. Frankland et al. [77] used molecular dynamics simulations to show that the nanotube/polymer interfacial shear strength can be enhanced by over an order of magnitude with the formation of cross-links involving less than 1% of the nanotube carbon atoms with negligible changes in the elastic modulus.

In their tailoring the interface of MWCNT/polymer composites, nanotube chemical modification, Eitan and co-workers [78] first attached carboxylic acid to the tube surface. This was followed by further reactions to attach di-glycidyl ether of bisphenol-A-based epoxide resin. It is then possible to further react the epoxide functional group to enable better interaction between the polymer matrix chains of the composite and the surface of the nanotube. Fig. 17 depicts the interface tailoring process and the resulting improvement in elastic modulus of unreinforced polycarbonate [79].

Gojny and co-workers [80,81] functionalized the nanotubes with amino acids by heating oxidized nanotubes with an excess triethylenetetramine. Their experimental results indicate that the introduced functional groups lead to covalent bonding of the nanotube surface with the epoxy resin. Upon expansion of matrix cracks through heating by the electron beam in the TEM, it is seen (Fig. 18) that the functionalized outer layer of

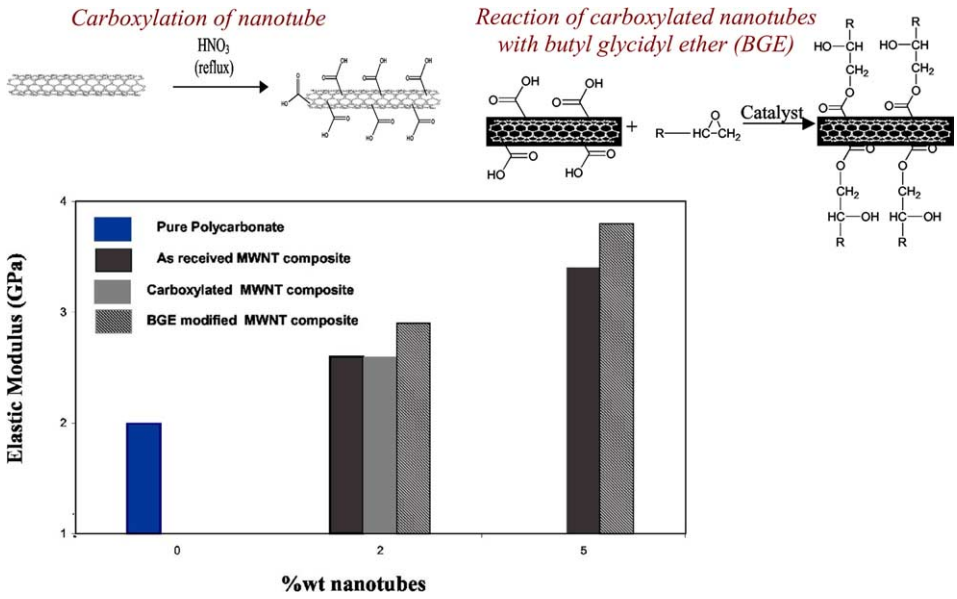

Fig. 17. Interface tailoring in polycarbonate/MWCNT composites and the resulting improvement in elastic modulus of unreinforced polycarbonate [79].

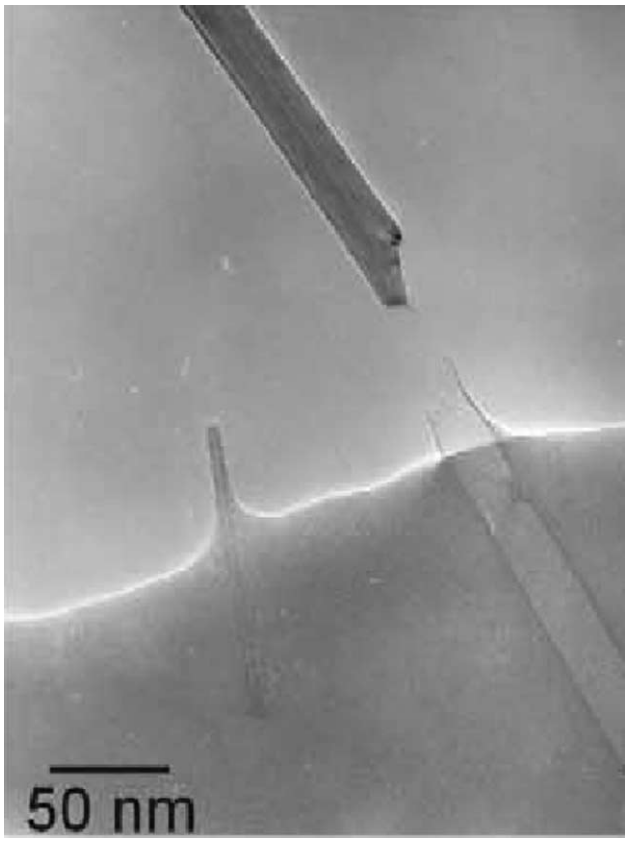

Fig. 18. Telescoping fracture of an amino acid functionalized multi-walled nanotube where the outer layer of the nanotube is still embedded in the matrix after fracture [81].

the multi-walled nanotube fractures and remains embedded in the epoxy matrix while the inner shells of the nanotube, which are bound together by the relatively weak van der Waals bonds, pull out in a sword-in-sheath mechanism.

Chemical functionalization of nanotubes can also be accomplished through irradiation with electrons or ions. Electron irradiation of carbon nanotubes causes their collapse in an anisotropic manner due to the knockout of atoms in the nanotube walls [72,82]. Ion deposition can induce cross-links between nanotubes in the bundle and between shells in MWNTs, which could lead to efficient load transfer among the tube layers.

Hu et al. [83] and Ni et al. [84] approached the modification of carbon nanotube/polystyrene composites through polyatomic ion beam deposition. Molecular dynamic simulations have demonstrated the modification of a composite of (10,10) SWCNT/polystyrene through the deposition of a beam of $C_3F_5^+$ polyatomic ions. Covalent cross-links were induced between otherwise un-functionalized SWCNT and a polystyrene matrix.

5.5. Modeling of transport and constitutive properties

The modeling of transport properties is illustrated by the work of Qunaies et al. [85] for the electrical behaviors of SWCNT/polyimide composites. The insulating nature of polyimides may cause significant accumulation of electrostatic charge on their surface, resulting in local heating and premature degradation to electronic components or space structures. Polyimide reinforced with SWCNT provides a level of electrical conductivity sufficient to permit electrostatic discharge as well as enhancement in thermal and mechanical properties. The percolation transition in CP2 polyimide/SWCNT composites was noticed between 0.02 and 0.1 vol% of

SWCNT; DC conductivity changed from 3×10^{-17} to 1.6×10^{-8} s/cm. The modeling predicts percolation concentrations of SWCNT in the vicinity of measured percolation threshold (0–0.2 vol%) for different SWCNT bundle size. Both analytical and characterization results lie between the single tube and seven tube arrangements, indicating that SWCNTs are dispersed in CP2 polyimide matrix as very thin bundles.

In the constitutive modeling of SWCNT/polymer composites [86–88], constitutive relationships for nanocomposites were developed as a function of the molecular structure of the polymer and nanotubes, and polymer/nanotube interface. In this approach, the molecular dynamics simulation was first used to obtain the equilibrium molecular structure, which consisted of a (6,6) SWCNT and five PmPV [poly(*m*-phenylenevinylene) substituted with octyloxy chains] oligomer, each 10 repeating units in length. Then a suitable representative volume element (RVE) of the nano-structure material is chosen. An equivalent-truss model of the RVE is developed as an intermediate step. The total strain energies in the molecular and equivalent-truss models, under identical loading conditions, are set equal. The nanotube, the local polymer near the nanotube, and the nanotube/polymer interface are then modeled as an effective continuum fiber by using an equivalent-continuum modeling. The effective fibers then serve as a means for incorporating micromechanical analyses for the prediction of bulk mechanical properties of SWCNT/polymer composites as functions of nanotube lengths, concentrations and orientations [86].

Pipes and Hubert [89,90] and Odegard et al. [91] adopted a self-similar approach to constitutive properties of SWCNT/polymer composites. There are three major steps in the modeling. First, a *helical array* of SWCNTs is assembled; and twisting the nanoarray (helical angle, 10°) provides an additional load transfer mechanism. Next, the nanoarrays are surrounded by a polymeric matrix and assembled into a second twisted array, *nanowire* with nanotube volume fraction of 54.6%. Lastly, the nanowires are impregnated with a polymer matrix and assembled into the final helical array, *micro-fiber* with nanotube volume fraction of 33.2%. The self-similar scheme, ranging from individual SWCNTs, nanoarray, nanowire to nanofiber is shown in Fig. 19. The self-similar approach and the equivalent-continuum modeling can predict elastic properties of the SWCNT/polymer composites in a combined range spanning from dilute to hyper-concentrated SWCNT volume fraction.

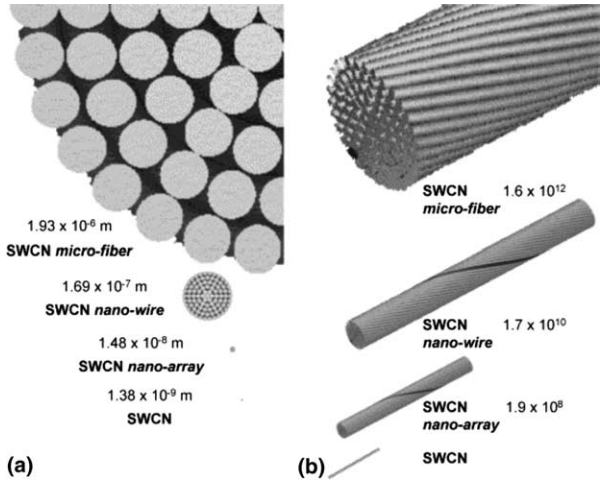

Fig. 19. Self-similar approach to constitutive properties of SWCNT/polymer [91].

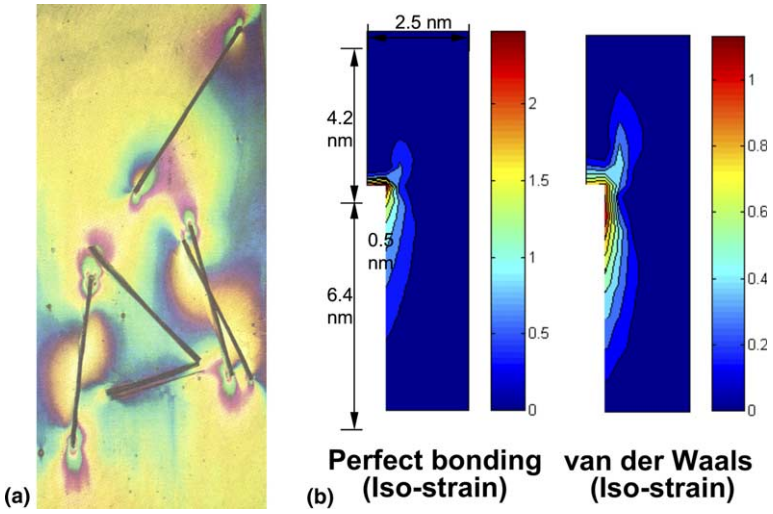

Fig. 20. (a) The photoelastic stress pattern of a short fiber/polymer composite [93] and (b) the shear stress distribution of a nanotube/polymer composite under axial tension using a multi-scale simulation [94].

6. Comparison of properties and performance

Although the length scales of reinforcements in nanocomposites, i.e., diameter of nanoparticles, diameter and length of nanofibers and nanotubes, as well as thickness of nanoplatelets are smaller than those of traditional composites by about three orders in magnitude, there are considerable differences and similarities in the properties and performance of nanocomposites and traditional fiber composites. It is highly desirable to present

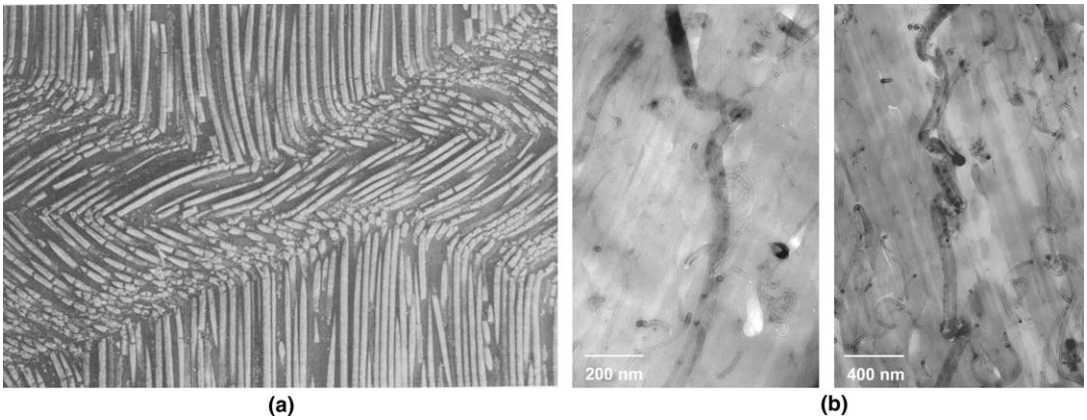

Fig. 21. (a) Slip band formation in a composite with Al_2O_3 fiber in an aluminum matrix [95] and (b) nanoscale buckling of carbon nanotubes in an aligned nanocomposite [96].

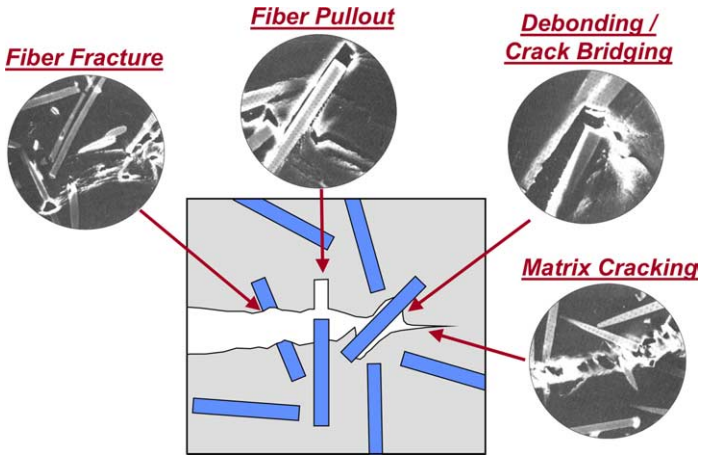

Fig. 22. Key mechanisms of energy dissipation have been identified in the fracture of short as well as continuous fiber-reinforced composites [93].

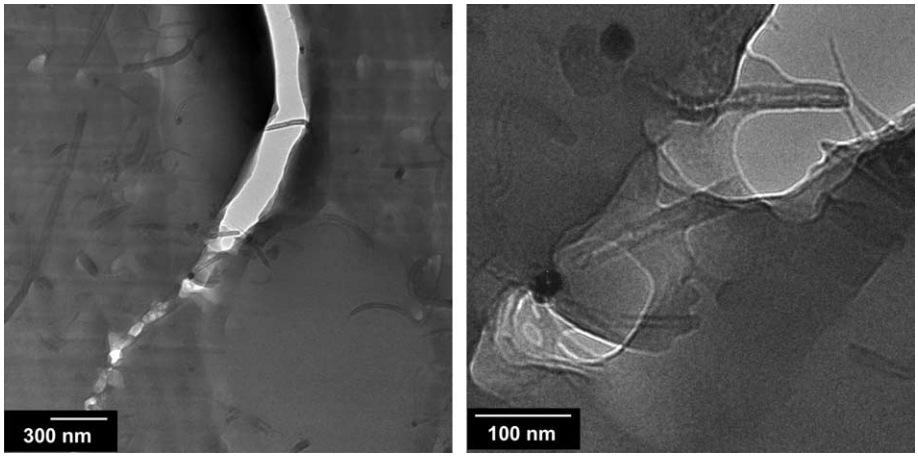

Fig. 23. Fracture mechanisms in carbon nanotube-reinforced composites [68].

some key properties of nanocomposites in contrast to the same properties in traditional composites, only a few examples are selected below.

It is well known in short-fiber composites that the presence of fiber-ends induces stress concentrations in the matrix materials when the composite is subjected to loading. The nature of stress concentration and the associated singularities have been studied in terms of the fiber bundle-end shape and bundle aspect ratio [92]. Fig. 20 compares (a) the photoelastic stress pattern of a short fiber/polymer composite [93] with the shear stress distribution of a nanotube/polymer composite under tension using a multi-scale simulation [94]. Two types of nanotube/matrix interfacial bonding conditions are considered. The length of nanotube is less than 1 nm whereas the short fibers are of millimeters in length. The general similarity in local stress concentration is unmistakable.

In the case of uniaxial compression of continuous fiber composite, it is well known that fiber defects or fiber misalignment may activate fiber bending and subsequent fiber buckling. Fig. 21(a) shows slip band formation in a composite with Al_2O_3 fiber in an aluminum matrix [95]. The activation and subsequent observation of nanotube buckling in a composite under compressive loading are much more difficult because of the small size and alignment of nanotubes. Thostenson and Chou [96] have succeeded in such experiments. The multiple buckling of individual MWCNTS in a polymer composite can be seen in Fig. 21(b). An atomistic modeling of elastic buckling of carbon nanotubes has been performed by Li and Chou [97].

Several key mechanisms of energy dissipation have been identified in the fracture of short as well as continuous fiber-reinforced composites. These are fiber fracture, fiber pullout, fiber/matrix debonding/crack bridging and matrix cracking. Fig. 22 shows schematically these mechanisms operating at a crack tip [93] as well as the micrographs demonstrating the individual failure modes. It is interesting to note that all these failure modes have also been observed in nanotube reinforced polymer composites as demonstrated by Thostenson and Chou [68] in Fig. 23.

One of the reasons of the recent enthusiasm toward carbon nanotubes as reinforcements for composite materials is their reported high elastic modulus and strength comparing to those of existing continuous fibers. The comparison is further demonstrated below. Fig. 24

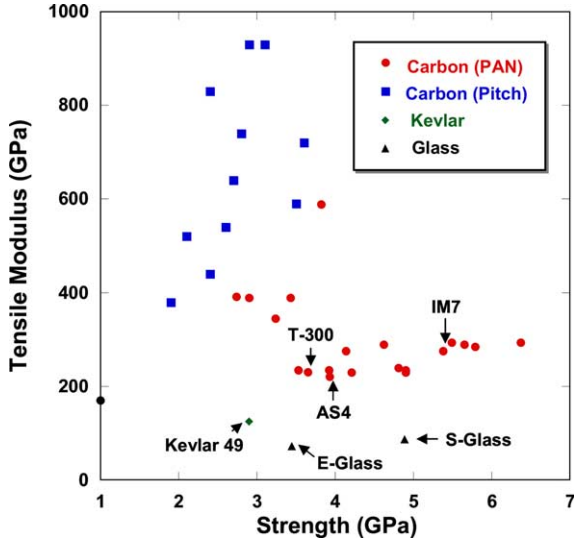

Fig. 24. Tensile modulus and strength of several major commercial fibers (data from Shindo [98]).

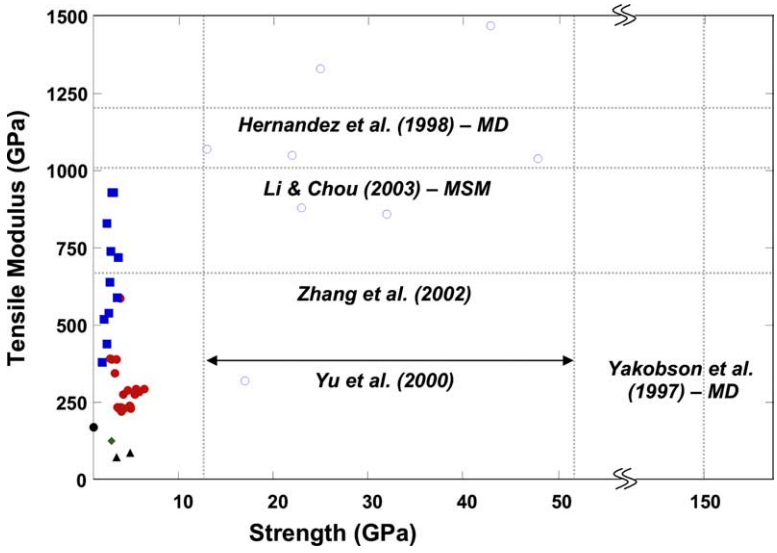

Fig. 25. Comparison of SWCNT properties with the properties of commercial fibers (Hernandez et al. [44]; Li and Chou [43]; Zhang et al. [99]; Yu et al. [57]; Yakobson et al. [59]).

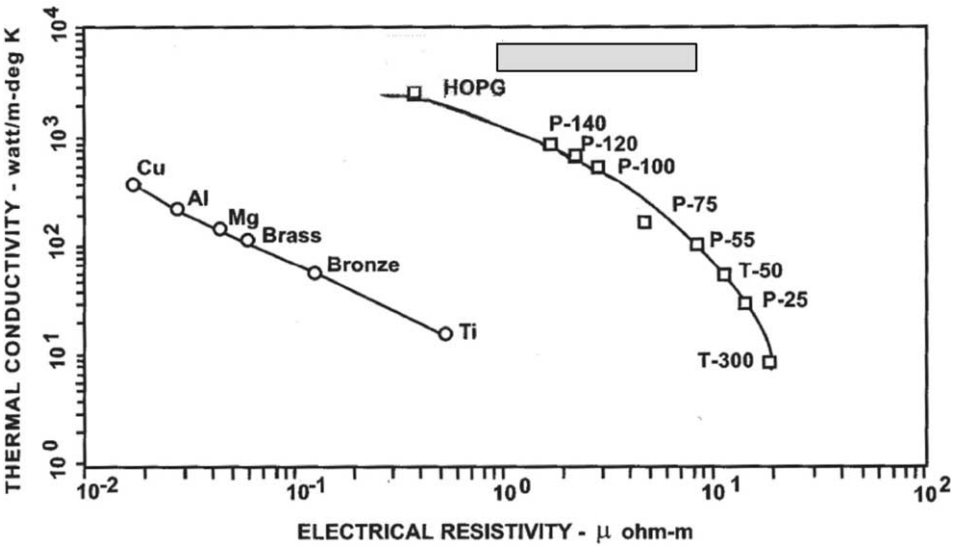

Fig. 26. Comparison of electrical resistivity and thermal conductivity [100]. Shaded region indicates the predicted carbon nanotube properties from [101–104].

summarizes the tensile modulus and strength of several major commercial fibers: PAN-based and pitched-based carbon fibers, Kevlar fiber and glass fiber [98]. A comparison of the fiber properties with those of SWCNTs is made in Fig. 25. Here, the experimental results of Yu et al. [57] are presented along with the modulus predictions of Hernandez et al. [44] using the tight-binding molecular dynamics, Li and Chou [43] using the molecular structural mechanics, and Zhang et al. [99] using a continuum approach. Because of the lack of corresponding strength data, these results of modulus predictions are indicated by horizontal lines. The range of measured strength data of Yu et al., denoted by the open circles, is indicated by two vertical lines. In addition, the strength predictions of Yakobson et al. [59] using molecular dynamics are indicated by a vertical line at 150 GPa.

Lastly, Fig. 26 shows the electrical resistivity and thermal conductivity of several bulk metallic materials (Cu, Al, Mg, brass, bronze, and Ti) as well as pitch carbon fibers (ranging from P-25 to P-140), PAN carbon fibers (T-300), and highly oriented pyrolytic graphite (HOPG) are given. The ranges of predicted electrical resistivity and thermal conductivity for SWCNTs are shown as the rectangular area in the top of Fig. 26 [100–104]. Because of the scattering in data of predicted electrical and thermal properties of SWCNTs, the results shown in Fig. 26 are understood not to be inclusive.

The addition of carbon nanotubes has been shown to significantly reduce the resistivity and percolation threshold in both polymer matrix materials, such as epoxy [105,106] and poly(butylene terephthalate) [107] as well as ceramic matrix materials, such as silicon carbide [108] and aluminum oxide [109].

7. Critical issues in nanocomposites

Just as in traditional fiber composites, the major challenges in the research of nanocomposites can be categorized in terms of the structures from nano to micro to macro levels. There is still considerable uncertainty in theoretical modeling and experimental characterization of the nano-scale reinforcement materials, particularly nanotubes. Then, there is a lack of understanding of the interfacial bonding between the reinforcements and the matrix material from both analytical and experimental viewpoints. Lastly, the challenges at the level of nanocomposites have mainly to do with the following issues related to composites processing:

7.1. Dispersion

Uniform dispersion of nanoparticles, and nanotubes against their agglomeration due to van der Waals bonding is the first step in the processing of nanocomposites. Beside the problems of agglomeration of nanoparticles, exfoliation of clays and graphitic layers are essential. SWCNTs tend to cluster into ropes and MWCNTs produced by chemical vapor deposition are often tangled together like spaghettis. The separation of nanotubes in a solvent or a matrix material is a prerequisite for aligning them.

7.2. Alignment

Because of their small sizes, it is exceedingly difficult to align the nanotubes in a polymeric matrix material in a manner accomplished in traditional short fiber com-

posites. The lack of control of their orientation diminishes the effectiveness of nanotube reinforcement in composites, whether for structural or functional performance.

7.3. Volume and rate

High volume and high rate fabrication is fundamental to manufacturing of nanocomposites as a commercially viable product. The lessons learned in the fabrication of traditional fiber composites have clearly demonstrated that the development of a science base for manufacturing is indispensable. Efficiency in manufacturing is pivotal to the future development of nanocomposites.

7.4. Cost effectiveness

Besides high volume and high rate production, the cost of nanocomposites also hinges on that of the nano-reinforcement material, particularly, nanotubes. It is anticipated that as applications for nanotubes and their composites increase the cost will be dramatically reduced.

8. Precursors for macroscopic composites

For substantially realizing their exciting potentials, robust processing and manufacturing methods are required to incorporate nano-reinforcements into macroscopic functional and structural composites. To utilize these nanostructured materials in engineering applications, it is crucial to develop processing techniques that are both scalable for producing macroscopic structures and capable of efficiently utilizing nanoscale reinforcement in the as-manufactured composite. Some promising techniques for processing precursors for macroscopic composites are briefly outlined in the following.

8.1. Long nanotube fibers and strands

Just as in traditional fiber composites, there has been strong impetus in producing "continuous" carbon nanotubes that will undoubtedly facilitate their structural and functional applications. Recent advances in processing long carbon nanotubes in the form of individual nanotubes and nanotube strands are briefly reviewed below.

First, Zheng et al. [110] have reported the synthesis of 4-cm-long individual SWCNTs by Fe-catalyzed decomposition of ethanol. In this process, a $FeCl_3$ solution was applied with a dip-pen to one end of the Si substrate, which was then placed in a horizontal quartz tube furnace with the catalyst end directed toward the gas flow, and ethanol vapor was then introduced into the furnace. The growth rate is 11 μm/s.

Zhu et al. [111] reported the direct synthesis of long strands of ordered SWCNTs by an optimized catalytic chemical vapor deposition with a floating catalyst method in a vertical furnace. A salient feature of this synthesis method is in the use of *n*-hexane in combination with thiophene and hydrogen, so large portions of long SWCNTs are formed and assembeled into macroscopic strands. SWCNT strands with a length of 20 cm and a diameter on the order of 0.3–0.5 mm have been accomplished. The tensile modulus of the strands is in the range of 49–77 GPa. The approximate volume fraction of nanotube in the strands, determined by analyzing the spacing between the nanotube ropes in the strands, is less than 48%. Hence, the tensile modulus based upon the net cross-section of the strand would be in the range of 100–150 GPa, consistent with the modulus of large SWCNT bundles.

Ericson et al. [112] recently reported the synthesis of macroscopic, neat SWCNT fibers. Because of the high-temperature stability of SWCNTs, wet spinning is the only viable approach, as is the case for conventional rod-like polymers such a PBO, PPTA and PBZT. The main challenge to the production of neat SWCNT fibers, according to Ericson et al. is dispersing the SWCNTs at high enough concentrations suitable for efficient alignment and coagulation. Davis et al. [113] have shown that SWCNTs can be dispersed at high concentrations in superacids. The functionalization of SWCNT sidewalls eliminated wall–wall van der Waals interactions and promotes their ordering into an aligned phase of individual mobile SWCNTs surrounded by acid anions. Then, using conventional fiber-spinning techniques, this ordered SWCNT dispersion could be extruded and coagulated in a controlled fashion to produce continuous lengths of macroscopic neat SWCNT fibers. Davis et al. [113] reported that the neat SWCNT fibers possess good mechanical properties, with a Young's modulus of 120 ± 10 GPa and a tensile strength of 116 ± 10 MPa. The electrical resistivity of the fibers is around 0.2 mΩ cm. The thermal conductivity of the either-coagulated fiber is 21 W/m K.

The process reviewed above for assembling carbon nanotubes into continuous fibers [111–113] have been achieved through post-processing methods. Li et al. [114] have reported the spinning of fibers and ribbons of carbon nanotubes directly from the chemical vapor deposition synthesis zone of a furnace using a liquid source of carbon and an iron nanocatalyst. The liquid feedstock is mixed with hydrogen and injected into the hot zone where an aerogel of nanotubes forms. This aerogel is captured and wound out of the hot zone continuously as a fiber or film (Fig. 27(a)). The wind-up assembly could operate at lower temperature outside the furnace hot zone (Fig. 27(b)). Fig. 27(c) shows that a permanent twist is introduced into a fiber that consists of well-aligned MWCNTs after its removal from the furnace.

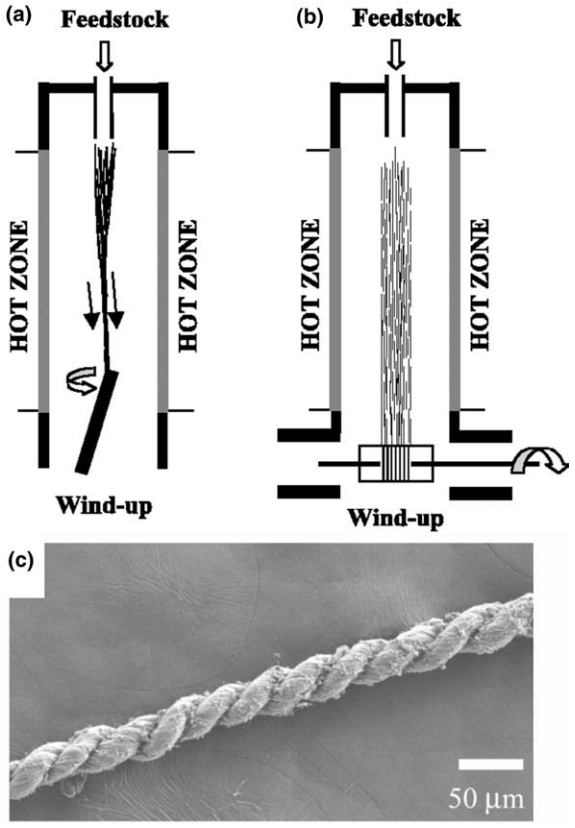

Fig. 27. Schematic of the direct spinning process where: (a) the wind-up is by an offset rotating spindle, (b) the wind-up assembly that operates at a lower temperature, outside the furnace hot zone and (c) SEM micrograph showing permanent twist introduced into a nanotube fiber from direct CVD spinning [114]. Reprinted with permission from [114]. Copyright (2004) AAAS.

The approach of coagulation-based carbon nanotube spinning was first developed by Vigolo et al. [115]. In this process, SWCNTs dispersed by a surfactant were injected through a needle or capillary tube using a syringe pump into co-flowing stream of polymer solution that contained 5 wt% of polyvinyl alcohol. Flow-induced alignment of the nanotubes took place at the tip of the capillary. The nanotube ribbons so formed could be drawn in the third dimension when the polymer solution was slowly pumped out from the bottom of the container. The needle or the capillary tube was oriented so that the SWCNT injection was tangential to the circular trajectory of the polymer solution in the container. Vigolo et al. [115] reported that the elastic modulus of the nanotube fibers is 10 times higher than the modulus of high-quality buckypaper.

By modifying the process of Vigolo et al. [115,116] and Poulin et al. [117], Dalton et al. [118] reported the conversion of gel fibers into long solid nanotube composite fiber in a continuous process at a rate of more than 70 cm/min. The resulting composite fibers are 50 μm in diameter, containing 60% SWCNTs. The fiber Young's modulus and tensile strength are 80 and 1.8 GPa, respectively. Large strain to failure was also recorded.

The concept of assembling SWCNTs into nano arrays, nanowires and finally, microfibers for modeling the constitutive properties of SWCNT/polymer composites [89–91] may have significant technological implications. If SWCNTs can be produced and controlled in a continuous manner, the resulting microfiber would represent the most efficient translation of the properties of nano-reinforcements to the microscopic and macroscopic level.

8.2. Multi-scale hybrid composites

8.2.1. Controlled growth of carbon nanotubes on fiber surfaces

The controlled surface growth of carbon nanotube is best illustrated by the work of Thostenson et al. [6] using carbon fibers. Fig. 1 demonstrates the reinforcement hierarchy in the multi-scale nanotube/fiber composites in which the woven fabric is deposited with nanotubes. Here, the length scales of structures encompass the macroscopic woven fabric (in meters), the microscopic carbon fibers (in microns) with nanotube growth, and individual nanotubes (in nanometers). It was concluded that carbon nanotubes at the fiber/matrix interface improved the interfacial shear strength because of local stiffening of the polymer matrix.

8.2.2. Nanoclay-enhanced matrix

Multi-scale hybrid composites have also been produced using nanoclay as reinforcement for the matrix material. The motivation of adding nanoclay to a resin matrix is for enhancing the resin stiffness. The benefits of such improvement have been demonstrated in the compressive strength of fiber composites, which is influenced by the matrix shear modulus. Subramaniyan and Sun [119] measured the off-axis compressive strength of S2 glass fiber ($V_f = 35\%$) reinforced vinyl ester resin with the addition of nanoclay particles. The improvement in

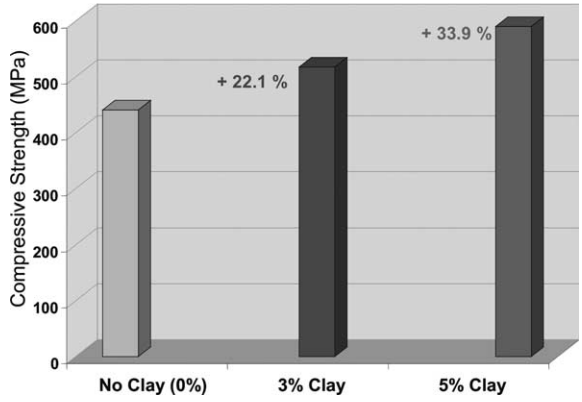

Fig. 28. Influence of nanoclay on the static compressive strength of S2 glass/vinyl ester composites [119].

compressive strength as shown in Fig. 28 is rather significant.

Liu et al. [120] synthesized a hybrid rubber-modified nanocomposite with organoclay. It has been demonstrated that organoclay enhances the degree of cure of the rubber-modified system as well as improves the fracture toughness, compression modulus, yield strength and ultimate strength of the epoxy resin.

8.2.3. Nanotube or nanofiber-reinforced matrix

Iwahori et al. [121] also pursued the concept of matrix modification by dispersing carbon nanofibers into the matrix of carbon fiber/polymer composites. They envisioned improvements in elastic modulus and resistance to crack propagation of the matrix phase and, consequently, its compressive strength and interlaminar strength.

Fig. 29 shows the experimental results of strength and modulus of carbon fiber woven fabric reinforced epoxy resin (EP 827®). The resin matrix is dispersed with a "cup-stacked" type carbon nano-fiber CARBERE® (CSNF), which is consisted of layers of truncated conical graphene sheets of diameter 80–100 nm and length < 1 μm (AR10) or <10 μm (AR50). Again, the addition of CSNF improves the matrix properties.

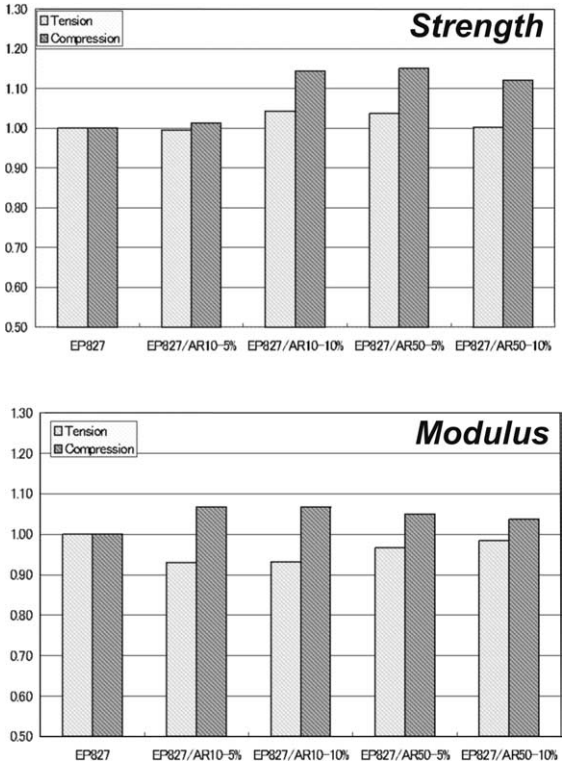

Fig. 29. Normalized mechanical properties of carbon nanofiber/carbon fiber hybrid composites [121].

8.3. Fibers and films

8.3.1. Nanocomposite fibrils

The potential for development of advanced continuous fibers with nanoscale diameter is attractive. Conventional mechanical spinning techniques are limited to producing fibers of micrometer diameters. As reviewed recently by Dzenis [122], electrospinning enables the production of polymer nanofibers from polymer solutions or melts in high electric fields. When the electric force on induced charges on the polymer liquid overcomes surface tension a thin polymer jet is ejected. The charged jet is elongated and accelerated by the electric field and can be deposited on a substrate. The potential of electrospun nanocomposite fibrils is exemplified below.

First, the work of Ko et al. [123] has demonstrated that continuous, PAN-based nanocomposite fibrils with SWCNT can be produced using electrospinning process. The alignment of SWCNTs in the fibril was achieved through flow and charge-induced orientation as well as confinement effect. Fig. 30 is a micrograph showing the alignment of nanotubes near the nozzle area. The composite fibril was carbonized at 750 °C and graphitized at 1100 °C in nitrogen environment.

Viculis et al. [124] have also utilized eletrospinning for studying the elastic properties of nanoplatelet/PAN nanocomposite fibrils. Here, graphite was intercalated with potassium to form the first stage intercalation compound, KC_8, and then exfoliated in aqueous solvents to produce graphite nanoplatelets. The nanoplatelets were then dispersed in a 7 wt% polyacrylonitrile (PAN) solution in *N*,*N*-dimethylformamide to form nanoscale fibrils by electrospinning. The elastic moduli of the nanocomposite fibrils have been measured by atomic force microscopy. The average moduli are 77.21, 112.69, 121.33, and 133.43 GPa, respectively, for nanoplatelet contents of 1, 2, 3, and 4 wt%. Three measurements were made at each nanoplatelet content. The

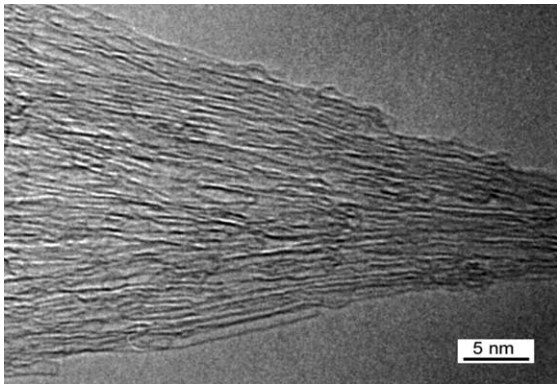

Fig. 30. PAN-based nanocomposite fibrils with SWCNT produced using the electrospinning process, showing alignment of the carbon nanotubes [123].

Table 7
PBO/SWCNT fiber properties [127]

Sample	Fiber diameter (μm)	Tensile modulus (GPa)	Strain to failure (%)	Tensile strength (GPa)	Compressive strength (GPa)
PBO	22 ± 2	138 ± 20	2.0 ± 0.2	2.6 ± 0.3	0.35 ± 0.6
PBO/SWNT (95/5)	25 ± 2	156 ± 20	2.3 ± 0.3	3.2 ± 0.3	0.40 ± 0.6
PBO/SWNT (95/5)	25 ± 2	167 ± 15	2.8 ± 0.3	4.2 ± 0.5	0.50 ± 0.6

goal of the work of Viculis et al. was to develop linear, planar and 3-D assemblies of the nanocomposite fibrils for macroscopic composites.

The electrospinning process has recently been utilized by Ko et al. [125] for the processing of carbon nanotube-reinforced spider silk. With strengths approaching 4 GPa and strain-to-failure exceeding 35%, spider silk has been recognized as a model of strong, tough fibers. Recent progress in biotechnology, notably by Nexia Biotechnologies through transgenic synthesis of spider silk polymer has enabled large-scale manufacturing of spider silk. In the process, recombinant spider silk, BIOSTEEL® in BELE® (Breed Early Lactate Early) goat system was produced in combination with pronuclear microinjection and nuclear transfer technologies resulting in a scalable manufacturing process for spider silk. In the work of Ko et al. [125], SWCNTs were successfully dispersed in transgenic spider silk with various combinations of silk proteins to form spinning dope for electrospinning. Nanofibers as small as 10 nm were co-electrospun to form aligned and random nanofiber assemblies. Initial tensile testing of the aligned silk composites showed a 10-fold increase in modulus, 5-fold increase in strength, and 3-fold increase in toughness with only 1 wt% of SWCNT in MaSpl silk matrix. These initial findings may have implications in a broad range of applications including tissue engineering scaffolds and ballistic armor.

Another example of the nanoparticle composite filament can be found in the work of Mahfuz et al. [126]. The reinforcement phase of the composite is a mixture of carbon particles (50–200 nm) and semi-crystalline whiskers (2–8 μm in diameter, 100–200 μm in length, 1.8 g/cm^3 density) produced by catalytic chemical vapor deposition. The matrix is a linear low density polyethylene (LLDPE). The processing of the nanocomposites involves the dry mixing of 2 wt% whisker and fine powder LLDPE followed by hot extrusion. The tensile modulus of nanocomposites in the filament direction is 270 MPa, a 16.37% gain comparing to the neat polyethylene modulus of 232 MPa. The nanocomposite tensile strength is 11.29 MPa as compared to 9.66 MPa for neat polyethylene.

Kumar et al. [127] have succeeded in demonstrating the enhancement in modulus, strength, and energy absorption of PBO/SWCNT composite fibers. In the process, Poly (*p*-phenylene benzobisoxazole) (PBO) was synthesized in the presence of SWCNT in poly (phosporic acid) (PPA) using typical PBO polymerization conditions. The SWCNTs were produced by the HiPco [128] process with an average diameter of about 0.95 nm. The PBO/SWCNT composite fibers were spun from the liquid crystalline solutions using dry-jet wet spinning. Table 7 summarizes the elastic and strength properties of the PBO/SWCNT composite fibers.

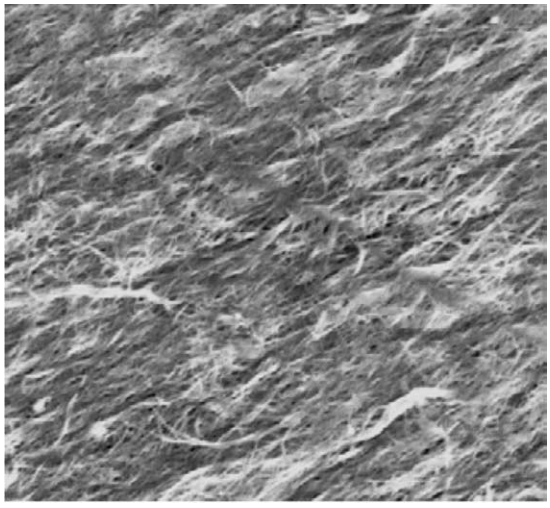

Fig. 31. Aligned nanotube bucky-papers [130].

8.3.2. Nanocomposite films

In addition to the creation of fibrils that can be used as potential fiber reinforcement in composites, the creation of large-scale nanocomposite films offers potential for the creation of macroscopic parts through the use of traditional composites manufacturing processes. For example, the method of Thostenson and Chou described in Section 5.3 results in a continuous ribbon of aligned nanocomposite that may then be laminated using traditional composites processing methods, such as autoclave molding or automated tape placement, to create macroscale aligned nanocomposites.

The approach of magnetically aligning SWCNTs was first given by Walters et al. [129]. Wang et al. [130] has demonstrated the high volume loading of SWCNT alignment in bucky paper using a stable SWCNT suspension prepared by sonicating a SWCNT/water/surfactant mixture. The filtration system was then placed inside the magnet bore and a bucky paper of 387 cm^2 (60 in.^{2}) × 17.8 μm was produced in 10 h under magnetic

fields of 17.3–25 Tesla (Fig. 31). Laminated composites were made by epoxy resin infiltration of stacked bucky papers with 59.8 wt% of SWCNT.

9. Concluding remarks

Recent advances in producing nanostructured materials with novel material properties have stimulated research to create macroscopic engineering materials by designing the structure at the nanoscale. Before these novel properties can be fully realized in a macroscopic composite, considerable basic research is necessary. The change in reinforcement scale poses new challenges in the development of processing as well as characterization techniques for these composites. The nano-meter scale of the reinforcement also presents additional challenges in mechanics research since we now must account for interactions at the atomic-scale.

Like all nanostructured materials, the properties of nanostructured composites are highly structure/size-dependent. To take the exceptional properties observed at the nanoscale and utilize these properties at the macroscale require a fundamental understanding of the properties and their interactions across various length scales. Ultimately a basic understanding of the structure-property relations will enable the nanoscale design of multi-functional materials for engineering applications ranging from structural and functional materials to biomaterials and beyond. Large-scale application of nanocomposites also requires the scale-up of manufacturing processes. Finally, there is a need to address the broad societal implications of nanotechnology of which nanocomposites is an important part.

Acknowledgments

This paper is dedicated to Professor A. Kelly.

The authors thank the support of the Air Force Office of Scientific Research (Grant No. F49620-02-1-0328 – Dr. Byung-Lip Lee, Program Director), the Army Research Office (Grant No. DAAD 19-02-1-0264 – Dr. Bruce LaMattina, Program Director), the National Science Foundation (NIRT Program, Grant No. 0304506, Dr. Ken P. Chong, Program Director), and the Office of Naval Research (Grant No. N0014-02-1-0960 – Dr. Ralph Wachter, Program Director).

References

[1] Kelly A. Composites in context. Compos Sci Technol 1985;23(3):171–99.
[2] Kelley A, Zweben C, editors. Comprehensive composite materials, vols. 1–6. Elsevier; 2000.
[3] American Ceramic Society (2004).
[4] Nanotechnology: Shaping the World Atom by Atom. National Science and Technology Council Interagency Working Group on Nanoscience, Engineering and Technology (1999). Available from: http://www.nano.gov.
[5] Thostenson ET. Carbon nanotube-reinforced composites: processing, characterization and modeling. Ph.D. Dissertation, University of Delaware; 2004.
[6] Thostenson ET, Li WZ, Wang DZ, Ren ZF, Chou TW. Carbon nanotube/carbon fiber hybrid multiscale composites. J Appl Phys 1998;91(9):6034–7.
[7] Thostenson ET, Chou TW. On the elastic properties of carbon nanotube-based composites: modeling and characterization. J Phys D 2003;36(5):573–82.
[8] Naganuma T, Kagawa Y. Effect of particle size on the optically transparent nano meter-order glass particle-dispersed epoxy matrix composites. Compos Sci Technol 2002;62(9):1187–9.
[9] Singh RP, Zhang M, Chan D. Toughening of a brittle thermosetting polymer: effects of reinforcement particle size and volume fraction. J Mater Sci 2002;37(4):781–8.
[10] Lopez L, Song BMK, Hahn HT. The effect of particle size in alumina nanocomposites. In: Proceedings of the 14th international conference on composite materials (ICCM-14), San Diego; 2003, Paper no. 138a.
[11] Thompson CM, Herring HM, Gates TS, Connell JW. Preparation and characterization of metal oxide/polyimide nanocomposites. Compos Sci Technol 2003;63(11):1591–8.
[12] Ash BJ, Siegel RW, Schadler LS. Mechanical behavior of alumina/poly (methyl methacrylate) nanocomposites. Macromolecules 2004;37(4):1358–69.
[13] Karger-Kocsis J, Zhang Z. Structure–property relationships in nanoparticle/semi-crystalline thermoplastic composites. In: Palta Calleja JF, Michler G, editors. Mechanical properties of polymers based on nanostructure and morphology. New York: Marcel Dekker Inc.; 2004.
[14] Luo JJ, Daniel IM. Characterization and modeling of mechanical behavior of polymer/clay nanocomposites. Compos Sci Technol 2003;63(11):1607–16.
[15] Krikorian V, Pochan DJ. Poly (L-lactic acid)/layered silicate nanocomposite: fabrication, characterization, and properties. Chem Mater 2003;15(22):4317–24.
[16] Gao F. Clay/polymer composites: the story. Mater Today 2004;7(11):50–5.
[17] Ray SS, Okamoto M. Polymer/layered silicate nanocomposites: a review from preparation to processing. Progr Polym Sci 2003;28(11):1539–641.
[18] Alexandre M, Dubois P. Polymer-layered silicate nanocomposites: preparation, properties and uses of a new class of materials. Mater Sci Eng R Rep 2000;28(1–2):1–63.
[19] Yasmin A, Abot JL, Daniel IM. Characterization of structure and mechanical behavior of clay/epoxy nanocomposites. In: Proceedings of the 14th international conference on composite materials (ICCM-14), San Diego; 2003, Paper no. 138(b).
[20] Okada A, Usuki A. The chemistry of polymer-clay hybrids. Mater Sci Eng C 1995;3(2):109–15.
[21] Miyagawa H, Drzal LT. Fracture behavior of epoxy/clay and epoxy/silica nanocomposites. In: Proceedings of the 14th international conference on composite materials (ICCM-14), San Diego; 2003, Paper no. 512a.
[22] Fukushima H. Drzal LT. Graphite nanocomposites: structural and electrical properties. In: Proceedings of the 14th international conference on composite materials (ICCM-14), San Diego; 2003, Paper no. 532a.
[23] Tsai J, Sun CT. Effect of platelet dispersion on the load transfer efficiency in nanoclay composites. J Compos Mater 2004;38(7):567–79.

[24] Ogasawara T, Ishida Y, Ishikawa T. Helium gas permeability of montmorillonite dispersed nanocomposites. In: Proceedings of the 11th US-Japan conference on composite materials, September 9–11 2004, Yonezawa, Yamagata, Japan.
[25] Zheng W, Wong SC. Electrical conductivity and dielectric properties of PMMA/expanded graphite composites. Compos Sci Technol 2003;63(2):225–35.
[26] Zheng W, Lu XH, Wong SC. Electrical and mechanical properties of expanded graphite-reinforced high-density polyethylene. J Appl Polym Sci 2004;91(5):2781–8.
[27] Song JH, Huh H, Hahn HT. Stress evaluation of nanocomposites with nanoplatelets. In: Proceedings of the 14th international conference on composite materials (ICCM-14), San Diego; 2003, Paper no. 512c.
[28] Merkulov VI, Lowndes DH, Wei YY, Eres G, Voelkl E. Patterned growth of individual and multiple vertically aligned carbon nanofibers. Appl Phys Lett 2000;76(24):3555–7.
[29] Endo M, Kim YA, Hayashi T, Fukai Y, Oshida K, Terrones M, et al. Structural characterization of cup-stacked-type nanofibers with an entirely hollow core. Appl Phys Lett 2002;80(7):1267–9.
[30] Endo M, Kim YA, Ezaka M, Osada K, Yanagisawa T, Hayashi T, et al. Selective and efficient impregnation of metal nanoparticles on cup-stacked-type carbon nanofibers. Nano Letters 2003;3(6):723–6.
[31] Wei CY, Srivastava D. Nanomechanics of carbon nanofibers: structural and elastic properties. Appl Phys Lett 2004;85(12):2208–10.
[32] Finegan IC, Tibbetts GG, Glasgow DG. Surface treatments for improving the mechanical properties of carbon nanofiber/thermoplastic composites. J Mater Sci 2003;38(16):3485–90.
[33] Finegan IC, Tibbetts GG, Gibson RF. Modeling and characterization of damping in carbon nanofiber/polypropylene composites. Compos Sci Technol 2003;63(11):1629–35.
[34] Ma HM, Zeng JJ, Realff ML, Kumar S, Schiraldi DA. Processing, structure, and properties of fibers from polyester/carbon nanofiber composites. Compos Sci Technol 2003;63(11):1617–28.
[35] Sandler J, Windle AH, Werner P, Altstadt V, Es MV, Shaffer MSP. Carbon-nanofibre-reinforced poly (ether ether ketone) fibres. J Mater Sci 2003;38(10):2135–41.
[36] Thostenson ET, Ren ZF, Chou TW. Advances in the science and technology of carbon nanotubes and their composites: a review. Compos Sci Technol 2001;61(13):1899–912.
[37] Iijima S. Helical microtubules of graphitic carbon. Nature 1991;354:56–8.
[38] Collins PG, Avouris P. Nanotubes for electronics. Scient Am 2000;283(6):62–9.
[39] Vaia RA, Wagner HD. Framework for nanocomposites. Mater Today 2004;7(11):33–7.
[40] Curtin WA, Sheldon BW. CNT-reinforced ceramics and metals. Mater Today 2004;7(11):44–9.
[41] Qian D, Wagner GJ, Liu WK, Yu MF, Ruoff RS. Mechanics of carbon nanotubes. Appl Mech Rev 2002;55:495–530.
[42] Srivastava D, Wei C, Cho K. Nanomechanics of carbon nanotubes and composites. Appl Mech Rev 2003;56(2):215–30.
[43] Li CY, Chou TW. A structural mechanics approach for the analysis of carbon nanotubes. Int J Solids Struct 2003;40:2487–99.
[44] Hernandez E, Goze C, Bernier P, Rubio A. Elastic properties of C and BxCyNz composite nanotubes. Phys Rev Lett 1998;80(20):4502–5.
[45] Lu JP. Elastic properties of carbon nanotubes and nanoropes. Phys Rev Lett 1997;79(7):1297–300.
[46] Krishnan A, Dujardin E, Ebbesen TW, Yianilos PN, Treacy MMJ. Young's modulus of single-walled nanotubes. Phys Rev B 1998;58(20):14013–9.
[47] Li CY, Chou TW. Elastic properties of single-walled carbon nanotubes in transverse directions. Phys Rev B 2004;84(1):121–3.
[48] Sanchez-Portal D, Artacho E, Soler JM, Rubio A, Ordejon P. Ab initio structural, elastic, and vibrational properties of carbon nanotubes. Phys Rev B 1999;59(19):12678–88.
[49] Chopra NG. Synthesis and characterization of B(x)C(y)N(z) nanotubes. Ph.D. Dissertation. University of California, Berkeley; 1996.
[50] Wong EW, Sheehan PE, Lieber CM. Nanobeam mechanics: elasticity, strength, and toughness of nanorods and nanotubes. Science 1997;277(5334):1971–5.
[51] Salvetat JP, Bonard JM, Thomson NH, Kulik AJ, Forro L, Benoit W, et al. Mechanical properties of carbon nanotubes. Appl Phys A 1997;69(3):255–60.
[52] Poncharal P, Wang ZL, Ugarte D, de Heer WA. Electrostatic deflections and electromechanical resonances of carbon nanotubes. Science 1999;283(5407):1513–6.
[53] Yu MF, Lourie O, Dyer M, Moloni K, Kelly T, Ruoff RS. Strength and breaking mechanism of multi-walled carbon nanotubes under tensile load. Science 2000;287:637–40.
[54] Demczyk BG, Wang YM, Cumings J, Hetman M, Han W, Zettl A, et al. Direct mechanical measurement of the tensile strength and elastic modulus of multiwalled carbon nanotubes. Mater Sci Eng A 2002;334(1–2):173–8.
[55] Bodily BH, Sun CT. Structural and equivalent continuum properties of single-walled carbon nanotubes. Int J Mater Product Technol 2003;18(4–6):381–97.
[56] Li CY, Chou TW. Elastic moduli of multi-walled carbon nanotubes and the effect of van der Waals forces. Compos Sci Technol 2003;63:1517.
[57] Yu MF, Files BS, Arepalli S, Ruoff RS. Tensile loading of ropes of single wall carbon nanotubes and their mechanical properties. Phys Rev Lett 2000;84(24):5552–5.
[58] Walters DA, Ericson LM, Casavant MJ, Liu J, Colbert DT, Smith KA, et al. Elastic strain of freely suspended single-wall carbon nanotube ropes. Appl Phys Lett 1999;74(25):3803–5.
[59] Yakobson BI, Campbell MP, Brabec CJ, Bernholc J. High strain rate fracture and C-chain unraveling in carbon nanotubes. Comput Mater Sci 1997;8(4):341–8.
[60] Belytschko T, Xiao SP, Schatz GC, Ruoff RS. Atomistic simulations of nanotube fracture. Phys Rev B 2002;65(23):235430.
[61] Li CY, Chou TW. Single-walled carbon nanotubes as ultrahigh frequency nanomechanical resonators. Phys Rev B 2003;68:073405.
[62] Li CY, Chou TW. Vibrational behavior of multi-walled carbon nanotube-based nanomechanical resonators. Appl Phys Lett 2004;84(1):121–3.
[63] Li CY, Chou TW. Mass detection using carbon nanotube-based nanomechanical resonators. Appl Phys Lett 2004;84(25):5246–8.
[64] Li CY, Chou TW. Strain and pressure sensing using single-walled carbon nanotubes. Nanotechnology 2004;15(11):1493–6.
[65] Tai NH, Yeh MK, Liu JH. Enhancement of the mechanical properties of carbon nanotube/phenolic composites using a carbon nanotube network as the reinforcement. Carbon 2004;42(12–13):2774–7.
[66] Gojny FH, Wichmann MHG, Köpke U, Fiedler B, Schulte K. Carbon nanotube-reinforced epoxy-composites: enhanced stiffness and fracture toughness at low nanotube content. Compos Sci Technol 2004;64(15):2363–71.
[67] Ogasawara T, Ishida Y, Ishikawa T, Yokota R. Characterization of multi-walled carbon nanotube/phenylethynyl terminated polyimide composites. Composites Part A 2004;35(1):67–74.
[68] Thostenson ET, Chou TW. Aligned multi-walled carbon nanotube-reinforced composites: processing and mechanical characterization. J Phys D 2002;35(16):L77–80.

[69] Frogley MD, Ravich D, Wagner HD. Mechanical properties of carbon nanoparticle-reinforced elastomers. Compos Sci Technol 2003;63(11):1647–54.
[70] NASA Tech Briefs, Mar-2004, p. 46, also NASA TSP MSC-23301 ''Elastomer Filled with Single-Wall Carbon Nanotubes''.
[71] Wagner HD, Vaia RA. Nanocomposites: issues at the interface. Mater Today 2004;7(11):38–42.
[72] Sinnott SB. Chemical functionalization of carbon nanotubes. J Nanosci Nanotechnol 2002;2(2):113–23.
[73] Liu J, Rinzler AG, Dai HJ, Hafner JH, Bradley RK, Boul PJ, et al. Fullerene pipes. Science 1998;280(5367):1253–6.
[74] Sen R, Zhao B, Perea D, Itkis ME, Hu H, Love J, et al. Preparation of single-walled carbon nanotube reinforced polystyrene and polyurethane nanofibers and membranes by electrospinning. Nano Letters 2004;4(3):459–64.
[75] Hamon MA, Hui H, Bhowmik P, Itkis HME, Haddon RC. Ester-functionalized soluble single-walled carbon nanotubes. Appl Phys A 2002;74(3):333–8.
[76] Chen RJ, Zhan YG, Wang DW, Dai HJ. Noncovalent sidewall functionalization of single-walled carbon nanotubes for protein immobilization. J Am Chem Soc 2001;123(16):3838–9.
[77] Frankland SJV, Caglar A, Brenner DW, Griebel M. Molecular simulation of the influence of chemical cross-links on the shear strength of carbon nanotube-polymer interfaces. J Phys Chem B 2002;106(12):3046–8.
[78] Eitan A, Jiang KY, Dukes D, Andrews R, Schadler LS. Surface modification of multiwalled carbon nanotubes: toward the tailoring of the interface in polymer composites. Chem Mater 2003;15(16):3198–201.
[79] Schadler LS, Jiang K, Andrews R, Eitan A. Nanotube reinforced polymer composites: tailoring the interface for improved mechanical properties. In: Proceedings of the 14th International conference on composite materials (ICCM-14), San Diego; 2003, Paper no. 422(b).
[80] Gojny FH, Schulte K. Functionalisation effect on the thermomechanical behaviour of multi-wall carbon nanotube/epoxy-composites. Compos Sci Technol 2004;64(15):2303–8.
[81] Gojny FH, Nastalczyk J, Roslaniec Z, Schulte K. Surface modified multi-walled carbon nanotubes in CNT/epoxy-composites. Chem Phys Lett 2003;370(5–6):820–4.
[82] Crespi VH, Chopra NG, Cohen ML, Zettl A, Radmilovic V. Site-selective radiation damage of collapsed carbon nanotubes. Appl Phys Lett 1998;73(17):2435–7.
[83] Hu Y, Jang I, Sinnott SB. Modification of carbon nanotube-polystyrene matrix composites through polyatomic-ion beam deposition: predictions from molecular dynamics simulations. Compos Sci Technol 2003;63(11):1663–9.
[84] Ni B, Andrews R, Jacques D, Qian D, Wijesundara MBJ, Choi YS, et al. A combined computational and experimental study of ion-beam modification of carbon nanotube bundles. J Phys Chem B 2001;105(51):12719–25.
[85] Qunaies Z, Park C, Wise KE, Siochi EJ, Harrison JS. Electrical properties of single wall carbon nanotube reinforced polyimide composites. Compos Sci Technol 2003;63(11):1637–46.
[86] Odegard GM, Gates TS, Wise KE, Park C, Siochi EJ. Constitutive modeling of nanotube-reinforced polymer composites. Compos Sci Technol 2003;63(11):1671–87.
[87] Frankland SJV, Harik VM, Odegard GM, Brenner DW, Gates TS. The stress–strain behavior of polymer-nanotube composites from molecular dynamics simulation. Compos Sci Technol 2003;63(11):1655–61.
[88] Saether E, Frankland SJV, Pipes RB. Transverse mechanical properties of single-walled carbon nanotube crystals. Part I: determination of elastic moduli. Compos Sci Technol 2003;63(11):1543–50.
[89] Pipes RB, Hubert P. Helical carbon nanotube arrays: thermal expansion. Compos Sci Technol 2003;63(11):1571–9.
[90] Pipes RB, Hubert P. Scale effects in carbon nanostrutures: self-similar analysis. Nano Letters 2003;3(2):239–43.
[91] Odegard GM, Pipes RB, Hubert P. Comparison of two models of SWCN polymer composites. Compos Sci Technol 2004;64(7–):1011–20.
[92] Chou TW. Microstructural design of fiber composites. Cambridge University Press; 1992.
[93] Chou TW, McCullough RL, Pipes RB. Composites. Scient Am 1986;254:193–203.
[94] Li CY, Chou TW. Multiscale modeling of carbon nanotube reinforced polymer composites. J Nanosci Nanotechnol 2003;3(5):423–30.
[95] Shetty HR, Chou TW. Mechanical-properties and failure characteristics of FP-aluminum and W-aluminum composites. Metall Trans A 1985;16(5):853–64.
[96] Thostenson ET, Chou TW. Nanotube buckling in aligned multi-wall carbon nanotube composites. Carbon 2004;42(14):3015–8.
[97] Li CY, Chou TW. Modeling of elastic buckling of carbon nanotubes by molecular structural mechanics approach. Mech Mater 2004;36(11):1047–55.
[98] Shindo A. Polyacrylonitrile (PAN)-based carbon fibers. In: Tsu-Wei Chou, vol. editor, Comprehensive composite materials. Elsevier; 2000, p. 1–33 [chapter 1.01].
[99] Zhang P, Huang Y, Geubelle PH, Klein PA, Hwang KC. The elastic modulus of single-wall carbon nanotubes: a continuum analysis incorporating interatomic potentials. Int J Solids Struct 2002;39(13-14):3893–906.
[100] Diefendorf RJ. Pitch precursor carbon fiber. In Tsu-Wei Chou, vol. editor, Comprehensive composite materials. Elsevier; 2000. p. 35–8 [chapter 1.02].
[101] Hone J, Whitney M, Piskoti C, Zettl A. Thermal conductivity of single-walled carbon nanotubes. Phys Rev B 1999;59(4):R2514–6.
[102] Hone J, Llaguno MC, Nemes NM, Johnson AT, Fischer JE, Walters DA, et al. Electrical and thermal transport properties of magnetically aligned single wall carbon nanotube films. Appl Phys Lett 2000;77(5):666–8.
[103] Berber S, Kwon YK, Tomanek D. Unusually high thermal conductivity of carbon nanotubes. Phys Rev Lett 2000;84(20):4613–6.
[104] Che JW, Cagin T, Goddard WA. Thermal conductivity of carbon nanotubes. Nanotechnology 2000;11(2):65–9.
[105] Martin CA, Sandler JKW, Shaffer MSP, Schwarz MK, Bauhofer W, Schulte K, et al. Formation of percolating networks in multi-wall carbon-nanotube–epoxy composites. Compos Sci Technol 2004;64(15):2309–16.
[106] Sandler J, Shaffer MSP, Prasse T, Bauhofer W, Schulte K, Windle AH. Development of a dispersion process for carbon nanotubes in an epoxy matrix and the resulting electrical properties. Polymer 1999;40(21):5967–71.
[107] Nogales A, Broza G, Roslaniec Z, Schulte K, Sics I, Hsiao BS, et al. Low percolation threshold in nanocomposites based on oxidized single wall carbon nanotubes and poly (butylene terephthalate). Macromolecules 2004;37(20):7669–72.
[108] Thostenson ET, Karandkiar PG, Chou TW. Fabrication and characterization of novel reaction bonded carbon nanotube-reinforced ceramic composites, submitted for publication, 2005.
[109] Zhan GD, Kuntz JD, Garay JE, Mukherjee AK. Electrical properties of nanoceramics reinforced with ropes of single-walled carbon nanotubes. Appl Phys Lett 2003;83(6):1228–30.
[110] Zheng LX, O'Connell MJ, Doorn SK, Liao XZ, Zhao YH, Akhadov EA, et al. Ultralong single-wall carbon nanotubes. Nature Mater 2004;3(10):673–6.
[111] Zhu HW, Xu CL, Wu DH, Wei BQ, Vajtai R, Ajayan PM. Direct synthesis of long single-walled carbon nanotube strands. Science 2002;296(5569):884–6.

[112] Ericson LM, Fan H, Peng HQ, Davis VA, Zhou W, Sulpizio J, et al. Macroscopic, neat, single-walled carbon nanotube fibers. Science 2004;305(5689):1447–50.
[113] Davis VA, Ericson LM, Parra-Vasquez ANG, Fan H, Wang YH, Prieto V, et al. Phase behavior and rheology of SWNTs in superacids. Macromolecules 2004;37(1):154–60.
[114] Li YL, Kinloch IA, Windle AH. Direct spinning of carbon nanotube fibers from chemical vapor deposition synthesis. Science 2004;304(5668):276–8.
[115] Vigolo B, Penicaud A, Coulon C, Sauder C, Pailler R, Journet C, et al. Macroscopic fibers and ribbons of oriented carbon nanotubes. Science 2000;290(5495):1331–4.
[116] Vigolo B, Poulin P, Lucas M, La76unois P, Bernier P. Improved structure and properties of single-wall carbon nanotube spun fibers. Appl Phys Lett 2002;81(7):1210–2.
[117] Poulin P, Vigolo B, Launois P. Films and fibers of oriented single wall nanotubes. Carbon 2002;40(10):1741–9.
[118] Dalton AB, Collins S, Munoz E, Razal JM, Ebron VH, Ferraris JP, et al. Super-tough carbon-nanotube fibres – these extraordinary composite fibres can be woven into electronic textiles. Nature 2003;423(6941):703–3.
[119] Subramaniyan AK, Sun CT. Enhancing the compressive strength of unidirectional polymeric composites using nanoclay. Composites Part A, 2005 [in press].
[120] Liu WP, Hoa SV, Pugh M. Morphology and performance of epoxy nanacomposites modified with organoclay and rubber. Polym Eng Sci 2004;44(6):1178–86.
[121] Iwahori Y, Ishiwata S, Ishikawa T. Mechanical properties of CFRP using CNF (Carbon Nano-Fiber) dispersed resin. In: Proceedings of the 14th international conference on composite materials (ICCM-14), San Diego; 2003, Paper no. 137a.
[122] Dzenis Y. Spinning continuous fibers for nanotechnology. Science 2004;304(5679):1917–9.
[123] Ko F, Gogotsi Y, Ali A, Naguib N, Ye HH, Yang GL, et al. Electrospinning of continuons carbon nanotube-filled nanofiber yarns. Adv Mater 2003;15(14):1161–5.
[124] Viculis L, Mack J, Ali A, Luoh R, Yang G, Kaner R, et al. Nanocomposite fibrils from graphite nanoplatelets. In: Proceedings of the 14th international conference on composite materials (ICCM-14), San Diego; 2003, Paper no. 138c.
[125] Ko FK, Gandhi1 M, Karatzas C. Carbon Nanotube Reinforced Spider Silk – A Model for the Next Generation of Super Strong and Tough Fibers. In: Proceedings of the 19th American society for composites annual technical conference, October 17–20; 2004, Atlanta, Georgia.
[126] Mahfuz H, Adnan A, Rangari VK, Jeelani S, Jang BZ. Carbon nanoparticles/whiskers reinforced composites and their tensile response. Composites Part A 2004;35(5):519–27.
[127] Kumar S, Dang TD, Arnold FE, Bhattacharyya AR, Min BG, Zhang XF, et al. Synthesis, structure, and properties of PBO/SWNT composites. Macromolecules 2002;35(24): 9039–43.
[128] Colbert DT, Smalley RE. Past, present and future of fullerent nanotubes: buckytubes. In: Osawa E, editor. Perspectives of fullerene nanotechnology. Kluwer Academic Publishers; 2002. p. 3–10.
[129] Walters DA, Casavant MJ, Qin XC, Huffman CB, Boul PJ, Ericson LM, et al. In-plane-aligned membranes of carbon nanotubes. Chem Phys Lett 2001;338(1):14–20.
[130] Wang B, Liang Z, Shankar KR, Barefield K, Zhang C, Kramer L. Fabrication and characterization of in-plane aligned nanotube composites with magnetically aligned carbon nanotube bucky papers. Proceedings of the 14th international conference on composite materials (ICCM-14), San Diego 2003; Paper no 422(a).